ELECTRICAL AND THERMAL EXPERIMENTAL CHARACTERIZATION AND MODELING OF CARBON NANOTUBE/EPOXY COMPOSITES

A Thesis

by

FRANK GARDEA

Submitted to the Office of Graduate Studies of
Texas A&M University
in partial fulfillment of the requirements for the degree of

MASTER OF SCIENCE

May 2011

Major Subject: Aerospace Engineering

Electrical and Thermal Experimental Characterization and Modeling of Carbon Nanotube/Epoxy Composites

ELECTRICAL AND THERMAL EXPERIMENTAL CHARACTERIZATION AND MODELING OF CARBON NANOTUBE/EPOXY COMPOSITES

A Thesis

by

FRANK GARDEA

Submitted to the Office of Graduate Studies of
Texas A&M University
in partial fulfillment of the requirements for the degree of

MASTER OF SCIENCE

Approved by:

Chair of Committee,	Dimitris C. Lagoudas
Committee Members,	James G. Boyd
	Hung-Jue Sue
Head of Department,	Dimitris C. Lagoudas

May 2011

Major Subject: Aerospace Engineering

ABSTRACT

Electrical and Thermal Experimental Characterization and Modeling of Carbon Nanotube/Epoxy Composites.

(May 2011)

Frank Gardea, B.S., Texas A&M University

Chair of Advisory Committee: Dr. Dimitris C. Lagoudas

The present work investigates the effect of carbon nanotube (CNT) inclusions on the electrical and thermal conductivity of a thermoset epoxy resin. The characterization of electrical and thermal conductivity of CNT/epoxy composites is presented. Pristine, oxidized, and fluorine-functionalized unpurified CNT mixtures ("XD grade") were dispersed in an epoxy matrix, and the effect of stirring rate and pre-curing of the epoxy on the dispersion of the CNTs was evaluated. In order to characterize the dispersion of the CNTs at different length scales, Optical Microscopy (OM), Raman Spectroscopy, and Scanning Electron Microscopy (SEM) was performed. Samples of varying CNT weight fractions were fabricated in order to find the effect of CNT weight fraction on thermal and electrical conductivity. Electrical conductivity was measured using a dielectric spectrometer, and thermal conductivity was determined by a transient plane source thermal analyzer.

It was found that electrical conductivity increases by orders of magnitude for the pristine and oxidized XD CNT composites relative to the neat epoxy matrix, while

fluorinated XD CNT composites remain electrically non-conductive. A small, but significant, increase in thermal conductivity was observed for pristine, oxidized, and fluorinated XD CNT composites, showing a linear increase in thermal conductivity with increasing CNT weight fraction. Pristine XD CNTs were ball-milled for different times in order to reduce the degree of agglomeration and entanglement of CNTs, and composites were fabricated using the same technique as with non-milled XD CNTs. Using ball-milled CNTs shows improved dispersion but results in an electrically non-conductive composite at the CNT weight fractions tested. The thermal conductivity of the ball-milled CNT samples shows an initial increase higher than that of non-milled pristine, oxidized, and fluorinated XD CNTs, but remains constant with increasing CNT weight fraction. A micromechanics model based on the composite cylinders method was implemented to model the electrical and thermal conductivity of the CNT/epoxy composites. Nanoscale effects in electrical and thermal conduction, such as electron hopping and interface thermal resistance, respectively, were incorporated into the model in order to accurately predict the acquired results. Modeling results show good agreement with acquired experimental results.

DEDICATION

I dedicate this work to myself

ACKNOWLEDGEMENTS

I would like to thank my committee chair and advisor, Dr. Dimitris C. Lagoudas, and my committee members, Dr. James G. Boyd and Dr. Hung-Jue Sue, for their time and guidance with this research.

I would also like to thank the United States Air Force AFRL Minority Leaders Program for providing me the opportunity to work on this research. I would especially like to thank Dr. Jennifer Chase Fielding and Dr. Merlin Theodore for their help and support. They increased my interest in science and provided me with the guidance and support necessary for success in this field of research.

I would like to extend my gratitude to Dr. Piyush Thakre and Patrick Klein for helping me since my undergraduate research and for teaching me the basic knowledge that was very helpful during my graduate research. I am personally grateful for the encouragement and advice Dr. Daniel C. Davis provided me at the beginning of my research and for motivating me to further expand my education. Also, thanks to Dr. Viktor Hadjiev and Dr. Amanda Young for all of their help with Raman Spectroscopy. I would also like to thank Dr. Zoubeida Ounaies and Sujay Deshmukh for their help with the electrical conductivity testing.

I would like to express my sincere gratitude to my dear friend Fang Dong. He constantly believed in me and was always there helping me move forward, and for that I am personally indebted to him. I cherish his friendship greatly.

One of the greatest motivations came from my siblings. I felt an obligation to continue my education in order for them to see me as a role model and continue in my footsteps. They have indirectly been a major source for my personal growth.

Lastly, I would especially like to thank my mother and father for their encouragement, support, and understanding. Their constant struggles and achievements have instilled knowledge in me and have been an inspiration both on a personal and professional level.

TABLE OF CONTENTS

LIST OF FIGURES

FIGURE Page

FIGURE Page

FIGURE Page

LIST OF TABLES

CHAPTER I

INTRODUCTION

The use of epoxy polymers has shown significant research interest due to their low density, ease of processability, and large range of applications [26,33,53,81,95]. However, the low electrical and thermal conductivity of epoxy presents performance limitations, specifically with thermal management and electrostatic discharge [67]. One way of increasing the low electrical and thermal conductivities of epoxy is by the incorporation of nanoscale particles, to create what are commonly referred to as nanocomposites [3,43,96]. Nanocomposites are multiphased materials where one of the phases has a dimension in the nanoscale (< 100 nm) [64]. The enhancement of the conductivity of epoxy has been pursued by embedding the polymer with nanoparticles with high thermal and electrical conductivity, in particular carbon nanotubes (CNTs) [67,91,95].

A. Background and Literature Review

The high aspect ratio and the high intrinsic electrical and thermal conductivity of CNTs should allow for a significant enhancement in the composite conductivity with only a minimal amount of dispersed CNTs [67]. In addition, due to their high strength and modulus [64], CNTs are a favorable candidate for developing a multifunctional composite material with enhanced mechanical and structural capabilities [45]. Altering

---

This thesis follows the style of International Journal of Engineering Science.

the low electrical and thermal conductivity of epoxy by the use of CNT inclusions gives the potential to control the conductivity of the composite by changing the CNT type, functionality, and weight fraction. In addition to thermal management and electrostatic discharge applications, other potential CNT/epoxy composite applications include the following: electrically insulating Thermal Interface Materials (TIM), where electrical isolation is required to prevent device interference while having heat dissipation, electrically conductive TIM where thermal performance and electrical connectivity is required, or as thermoelectric materials, where a high electrical conductivity is needed with low thermal conductivity [49,85,91].

In 1991, Iijima discovered carbon with a cylindrical structure after analyzing carbon deposit on an electrode [22]. Carbon nanotubes can be visualized as rolled sheets of graphene [47]. A single-wall carbon nanotube (SWCNT) consists of a single graphene cylinder [47] whereas a multi-wall nanotube (MWCNT) consists of multiple concentric graphene cylinders [22]. CNTs can have diameters of 0.4 to 100 nm, with lengths in the order of micrometers [64], resulting in very large aspect ratios, or length to diameter ratios. As a result of this large aspect ratio, CNTs can be considered one-dimensional. The one-dimensional structure gives rise to very unique properties.

CNTs are highly electrically conductive, reaching experimentally verified electrical conductivities on the order of 1000-2000 S/cm [44]. Electrical resistance in a CNT arises from the deflection of an electron from its mean free path, either due to defects or electron collisions [47,99]. The high aspect ratio present in CNTs allows for scattering to be less likely, due to the restriction on the electrons to travel only in one

dimension. The lack of electron scattering in defect free CNTs facilitates the flow of electrons through the material and hence a high electrical conductivity results [47,99].

Theoretical and experimental results have shown that CNTs have large intrinsic thermal conductivity values. Theoretical studies have yielded the axial thermal conductivity of an individual SWCNT close to 6600 W/mK [7] while experimental tests performed on MWCNT have shown a thermal conductivity of up to 3000 W/mK [50]. The one-dimensional structure of CNTs allows for phonons to travel along a mean free path [75] with minimal scattering, if the CNT has minimal defects [99]. The non-scatter of the phonons, along with the rigidity of the tube, allows for the high intrinsic thermal conductivity in CNTs along the tube axis [7].

Many efforts have been made to obtain well-dispersed CNTs in a polymer matrix. The focus on improving CNT dispersion arises from the finding that well dispersed CNTs can improve properties of polymer composites [59,68,108]. One fabrication method used to disperse CNTs is by solution blending. This procedure involves dispersing CNT in a solvent either by ultrasonication or by shear mixing, mixing the CNT/solvent solution with the polymer, and obtaining a composite by precipitating or casting a film [68]. One difficulty with solution blending is the tendency for the CNTs to agglomerate during solvent evaporation. Chemically-treated CNTs can enable more stable solutions [13,20], and improve CNT dispersion when using solution blending [33,68]. Another method of dispersion is using surfactants with a solution blending technique to obtain exfoliated CNTs. One problem with this technique is that the surfactant remains in the composite, which might affect the properties of the

composite [68]. Another nanocomposite fabrication technique is melt blending. Melt blending utilizes high temperature and high shear forces to disperse the CNTs in the matrix, usually with thermoplastic polymers [33,68]. In situ polymerization is also used, where the CNTs are first dispersed in a monomer followed by polymerization. Some processing has been done at very high viscosities, such as solid-state mechanochemical pulverization, in order to possibly graft the polymer to the CNTs [68]. Another method that produces uniform dispersion of CNTs is a latex fabrication method. This method adds latex nanoparticles to a CNT/water suspension. After freeze drying and additional processing, a composite with uniform CNT dispersion results [68].

Many studies have been performed on the electrical [5,47] and thermal conductivity [107] of CNT composites. Sandler et al. showed that the percolation threshold (the concentration at which a conductive network is formed within the matrix) of CNT/epoxy composites depends greatly on the degree of dispersion of the nanotubes. They obtained ultra-low percolation thresholds by growing aligned CNTs before shear mixing with epoxy, instead of mixing entangled CNTs [80]. Even though percolation was achieved at a weight fraction of 0.0025wt%, it is most likely due to percolation of large aggregates present in the samples and not by percolation of individual tubes, since the focus was to induce the formation of CNT clusters to form an electrically conductive network [80]. Martin et al. concluded that the dielectric behavior on CNT composites depends greatly on the processing conditions [65]. The aim of [65] was not to obtain exfoliated CNTs but to control the agglomeration process and enhance agglomeration in order to reach lower percolation thresholds. The use of SWCNT has shown significant

improvement in electrical conductivity up to about 9 or 10 orders of magnitude at CNT weight fractions of only 0.1-0.2wt% [72,95]. Gojny et al. found that electrical conductivity and percolation threshold of CNT/epoxy composites is influenced by aspect ratio, dispersibility, and surface functionality [28]. They found that the percolation threshold is inversely proportional to the aspect ratio, and thus any treatment that reduces the CNT length, such as chemical functionalization [57] or ultrasonication, will result in an increase in percolation threshold. Li et al. found that, in addition to aspect ratio, the percolation threshold depends on the disentanglement of CNT agglomerates and the uniform dispersion of individual CNTs or CNT agglomerates, with lower percolation thresholds with loosely entangled and uniformly dispersed CNT agglomerates [54]. It has been shown, by Kim et al., that chemically modifying the CNT wall has a significant detrimental effect on the electrical conductivity of the nanocomposite, showing a decrease in electrical conductivity, at low weight fractions, of 2-3 orders of magnitude and an increase in percolation threshold up to a factor of 3, depending on the degree of functionalization [51]. Ramasubramaniam et al. found that the dispersion of non-covalent functionalized SWCNTs in polystyrene or polycarbonate can increase the electrical conductivity up to 14 and 15 orders of magnitude relative to the neat polymer, respectively [78]. The percolation threshold was found to be higher for polycarbonate, 0.11 wt% SWCNT, than for polystyrene, 0.045wt% SWCNT, showing that electrical conductivity and percolation threshold might depend on the host matrix properties [78,107]. Smith et al. [92], along with Curran et al. [15], have suggested that the electrical conductivity of CNT nanocomposites is due to an electron

hopping conduction mechanism between adjacent tubes. Charge transport in CNT composites is dominated by the hopping of electrons from one conductive site to the other [15,76]. The transport of charge carriers between CNTs is determined by the CNT to CNT separation, along with the thickness of the polymer coating around the CNT [92].

Some SWCNT/epoxy composites have shown an increase of 125% and higher in thermal conductivity, at room temperature, with a CNT weight fraction of 1.0 wt% [8,18], while others have shown minimal improvements in thermal conductivity with CNT weight fraction using SWCNT, MWCNT, or functionalized CNTs [28,40]. Moisala et al. show that SWCNT/epoxy composites show a decrease in thermal conductivity with increasing weight fraction, relative to the neat epoxy, even though the same composites are electrically conductive [67]. They attribute this result to either defective CNTs or to a large interface thermal resistance between the CNT and the epoxy. Phonons, "propagating vibration of waves responsible for thermal transport" [88], dominate thermal conduction in CNT composites. A large thermal interface resistance arises from weak coupling of phonons between the CNT and the matrix [67]. Since there is a large difference in stiffness between the CNTs and the polymer matrix [67], there is a difference in the frequency of phonon vibrations between the two phases [88,107]. This mismatch in vibration frequency gives rise to the large interfacial resistance to heat flow [107]. Song et al. found that the interfacial thermal resistance in a CNT composite can be reduced by decreasing the length and degree of entanglement

of the CNTs [93]. They increased the thermal conductivity of CNT/glycerin and CNT/silicone composites by about 55 and 147%, respectively, with shorter CNTs.

Computational methods have also been used to predict the electrical and thermal conductivity of CNT composites. Monte Carlo simulations performed by Foygel et al. show that the percolation threshold is inversely proportional to the aspect ratio of the filler [25]. Also, they found that the critical volume fraction required to achieve percolation is of the order of 0.01% for an aspect ratio of 2000. Deng et al. developed an analytical model for predicting the effective electrical conductivity of CNT composites by not only considering volume fraction and percolation, but by including the CNT anisotropy and non-straightness [16]. They found that curvature in a CNT greatly influences the effective electrical conductivity of the composite. Seidel et al. used a micromechanics approach, using composite cylinders, to find the effects of electron hopping on the percolation threshold and electrical conductivity of CNT nanocomposites [82]. Molecular dynamics simulations were used by Shenogin et al. to demonstrate how the thermal interface resistance between a CNT and an octane liquid greatly affects the heat flow [88]. They state the thermal conductivity of CNT/polymer composites will be limited by the presence of this interface resistance. Chen et al. simulated the effective thermal conductivity of CNT composites by modeling the CNTs as springs in series and in parallel [12]. They found that the interface thermal resistance on the lateral surfaces is not as significant as the thermal resistance at the nanotube ends.

B. Objectives and Outline of Present Work

The proposed work aims at investigating the electrical and thermal conductivity of carbon nanotube/epoxy composites. The effect of stirring rate and the degree of pre-curing of the epoxy on XD CNT dispersion will be determined by varying these fabrication parameters. Also, by introducing functionalities to the XD CNT walls, the effect of functionality on both electrical and thermal conductivity will be analyzed. The conductivities of these composites will then be determined experimentally as a function of filler concentration. An understanding of the conduction mechanisms present in XD CNTs embedded in the epoxy matrix will be pursued by the use of computational modeling. The modeling of a CNT/epoxy composite will provide the knowledge for the improvement or reduction of the electrical and thermal transport properties by incorporating nanoscale conduction mechanisms into the composite cylinder model.

In this work, Chapter II presents the methodology used, both experimental and theoretical. In the experimental part, the materials and fabrication method used for the nanocomposite plates will be presented. Also, the morphological, electrical, and thermal characterization methods will be described. A detailed description of the micromechanics modeling of electrical and thermal conductivities of CNT/epoxy composites is provided in the theoretical methodology. Chapter III begins with the characterization of the CNT material. This chapter mainly focuses on the experimental results of the dispersion analysis and the experimental and theoretical results of the electrical and thermal characterization. Finally, Chapter IV summarizes the conclusions

of this study, and recommends actions for future work on the characterization of CNT/epoxy composites.

CHAPTER II

METHODOLOGY

This chapter presents the methods used in order to accomplish the objectives of this research. The techniques used for obtaining both experimental and theoretical results are introduced. The materials used, along with the procedure for fabricating CNT/epoxy composites, are described. The tools used for the characterization of the CNT/epoxy composites are also presented. Finally, the micromechanics modeling approach is outlined.

A. Experimental

1. Materials

The epoxy resin, EPON^{TM} 862, and curing agent, EPIKURE^{TM} W, used in this study were both obtained from Hexion Specialty Chemicals, Inc. EPON^{TM} 862 is a diglycidyl ether of bisphenol F type resin with low viscosity and a density of 1.2 g/cm^3 [36]. EPIKURE^{TM} W is a low viscosity aromatic amine with a density of 1.02 g/cm^3 [35]. EPON^{TM} 862 can be cross-linked with the EPIKURE^{TM} W curing agent at a proportion of 100:26.4 by weight to obtain good mechanical and adhesive properties, along with high electrical and thermal resistance [36]. The nanoconstituents used are carbon nanotubes (XD CNTs) obtained from Carbon Nanotechnologies, Inc. (now Unidym, Incorporated). This grade (XD) of CNTs contains mostly single-wall CNTs [95,105].

The supplied pristine XD CNT material consists of micrometer size aggregates (bundles) as seen in Figure 1(a). The XD CNTs have aspect ratios greater than 1000 [105].

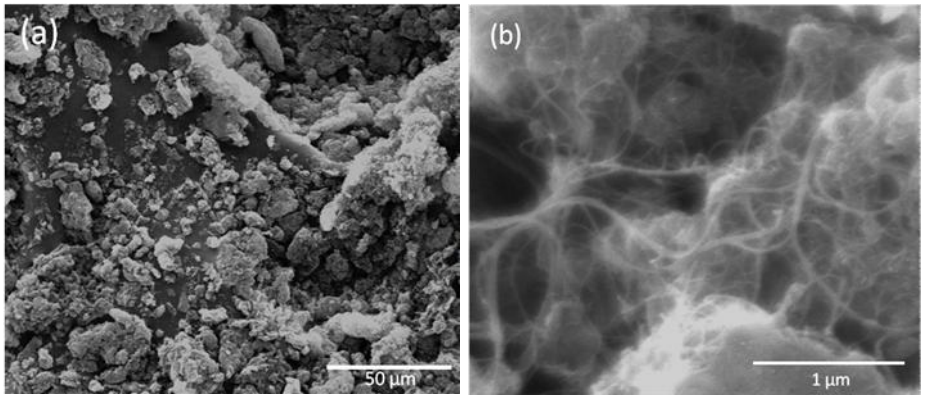

Figure 1. SEM images of pristine XD CNT bundles (a) 800X (b) 50000X

It has been shown that the addition of covalent functionalization to the CNTs improves CNT dispersion as a result of improved interaction with the matrix [21,24,27,37,77,86,100,104,113]. Thus, in order to possibly improve the dispersion of these XD CNTs in the epoxy, a sidewall covalent functionalization can be used.

The oxidation of XD CNTs was performed using a variation of the procedure from Warren et al. [105]. A total of one gram of XD CNTs was oxidized. A total of 120 ml of H_2SO_4/HNO_3, at a ratio of 3:1, was mixed for 10 minutes in a flask and then the total amount of XD CNTs added. The XD CNT/acid solution was ultrasonicated at 40 kHz for 2.5 hrs in an ultrasonic bath. After ultrasonication, 380 ml of deionized water was poured into the XD CNT/acid solution and ultrasonicated for an additional 3 hours. The

solution was vacuum filtered and the filter paper washed with 200 ml of deionized water in a separate beaker. The filtration and washing was repeated until the solution was neutralized. The washed XD CNTs on the filter paper were then placed in acetone and filtered again. The final oxidized XD CNTs were placed in an oven for 24 hours at 60 °C, under vacuum, in order to evaporate the solvent.

This oxidation adds a carboxylic acid group to the surface of the XD CNTs as shown in the schematic in Figure 2, which should result in improved bonding with the matrix [51,113]. Fluorine functionalized [66] XD CNTs were obtained from Rice University.

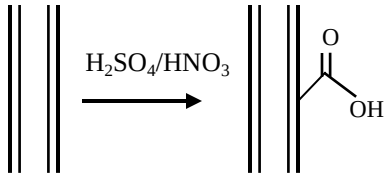

Figure 2. Schematic of oxidation of XD CNT

An SEM image of the final oxidized XD CNT bundles is shown in Figure 3(a) and an image of the supplied fluorinated XD CNT bundles is shown in Figure 3(b).

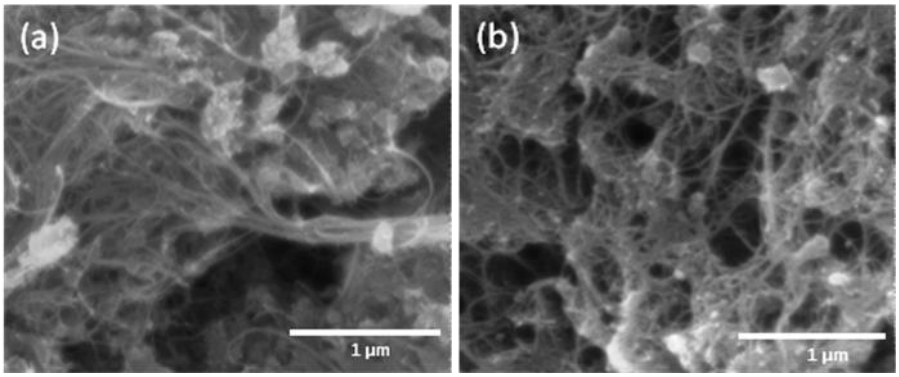

Figure 3. SEM image of (a) oxidized XD CNT bundles (b) fluorinated XD CNT bundles

It has been shown that mechanically ball-milling CNTs effectively reduces the degree of entanglement and length of CNTs [1,74]. Therefore, CNTs were ball-milled using a high energy SPEX SamplePrep 8000M Mixer/Mill in order to reduce the CNT length, along with breaking up the large aggregates present. Two different ball-milling times, 5 and 10 minutes, were done with a total of 1 gram of XD CNTs for each milling time. Fifteen stainless steel balls with a 0.375 in. diameter and 35 balls with a 0.25 in. diameter, with a total weight of 89.10 g, were used for the milling, along with a stainless steel container.

2. Nanocomposite Fabrication

The dispersion of CNTs in a polymer matrix can be controlled by varying fabrication parameters such as stirring rate, curing temperature, and rate of curing [65]. In order to study the effect of stirring rate and curing on CNT/epoxy composites, a base fabrication procedure obtained from Thakre et al. [95] was modified to improve CNT dispersion. The base fabrication procedure used is as follows. Carbon nanotubes were

ground in 2 ml of ethanol with a mortar and pestle until all large particles were broken into smaller particles. The CNT bundles were then dispersed, in a flask, in a mixture of 15 ml of toluene and 25 ml of ethanol with an ultrasonicator bath at 40 kHz. The ultrasonication was performed for 1 hour, and immediately after, the nanotube/solvent solution was added to the EPON 862 resin at 60 °C. Magnetic stirring was done at 60 rpm until all the solvent evaporated. In order to increase the rate of evaporation, a vacuum pump and cold trap set up was used. Once all the solvent evaporated, the appropriate amount of curing agent was added and stirred at 60 rpm at 60 °C. The solution was then degassed using a vacuum pump in order to remove any air bubbles. The solution was then poured into a glass mold and cured for 2 hours at 120 °C followed by additional curing at 175 °C for 2 hours.

In order to study the effect of stirring on the dispersion of XD CNTs, the stirring rate during solvent evaporation was varied from 60 rpm to 400 rpm while keeping all other steps in the base fabrication procedure constant.

To increase the viscosity of the solution, and thus enhance the effectiveness of the stirring [65], by the presence of higher shear forces [80], and reduce the movement of CNTs during curing, the epoxy was pre-cured with 20% of the total amount of the curing agent, at 120 °C, to the CNT/epoxy solution, once the solvent was removed. All other steps where kept the same. Pre-curing times of 0, 180, and 200 minutes were used. Following the pre-curing, the solution was first cooled to about 80 °C in order to increase its viscosity and then the remaining amount of curing agent was added and degassed at 400 rpm for 30 minutes. The solution was further cooled to about 60 °C, in

order to further increase its viscosity, and degassed for another 15 minutes at 400 rpm. The CNT/epoxy solution was then poured into a 40 °C pre-heated mold and placed in an oven. The curing cycle was set to 8 hrs at 40 °C followed by 2 hrs at 122 °C and another 2 hrs at 177 °C. Because the resin viscosity decreases with increasing temperature, the slow curing of 8 hrs at 40 °C was intended to slowly continue increasing the viscosity of the solution before curing at a higher temperature where CNT movement is more probable, thus preventing severe agglomeration.

3. Morphological Characterization

Optical microscopy was performed using an Olympus SZX16 microscope. Transmitted light was used to illuminate the sample through the thickness and thus analyze the dispersion of the CNTs within the sample and not just the surface. Images were taken at multiple magnifications for each sample fabricated. No sample preparation was required.

In order to analyze the distribution and uniformity of the dispersion of CNTs at the micrometer scale, Raman spectroscopy was performed using a Horiba Jobin-Yvon LabRam Raman Confocal Microscope. By measuring the Raman active atomic vibrations of the CNTs, it becomes possible to construct an image of the spatial distribution of the CNTs in the epoxy matrix [19,31,32]. By scanning a laser beam over an area on the composite sample as shown in Figure 4 [31], an image can be obtained from the intensity of the Raman spectrum at each step of the scan. Thus, the final image will include the distribution of the Raman intensity of certain CNT vibrations, yielding a

qualitative assessment of the distribution of CNTs in the matrix. The Raman active vibrations of a CNT are shown in Figure 5 [31].

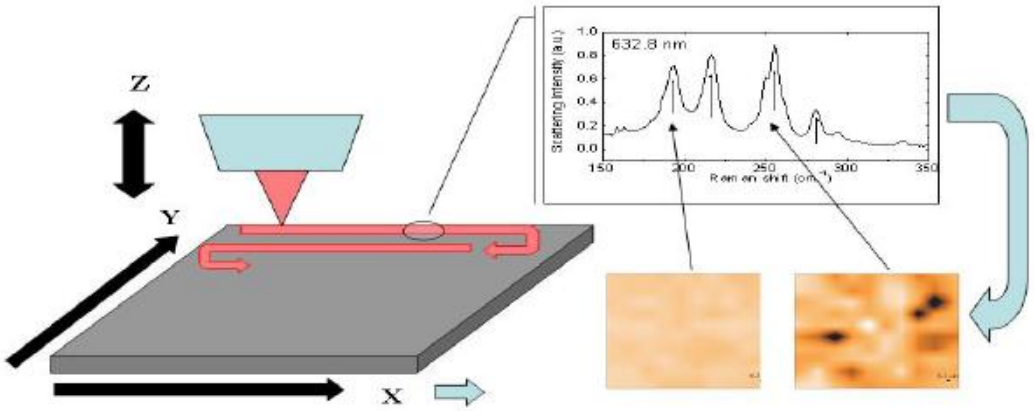

Figure 4. Schematic of scanning technique used to obtain a Raman image [31]

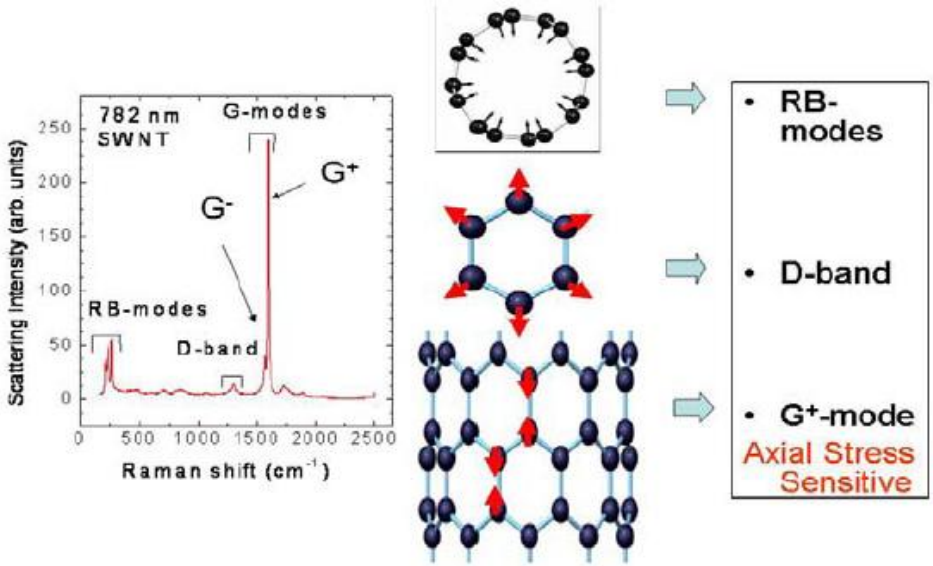

Figure 5. Raman active vibrations in a carbon nanotube [31]

The radial breathing (RB) mode, which corresponds to atom vibrations perpendicular to the CNT axis, is observed between 100 and 300 cm^{-1}. The RB mode is related to the diameter of the CNT. The D-band is a measure of the disorder in the CNT and the corresponding Raman shift ranges from 1290-1360 cm^{-1}. The D-band is activated by the breaking of symmetry in the crystalline structure of a CNT [112]. In other words, it can be related to defects in the CNT along with covalent functionalization of the CNT [31,112]. The tangential C-C stretching vibrations in a CNT are the G-modes and have frequencies in the range of 1520-1600 cm^{-1}. The G-mode is related to the strain in a CNT and to whether the CNT is metallic or semiconducting [31].

Raman spectroscopy was performed on each test specimen using a 785 nm laser focused with a 50X microscope objective with no required sample preparation. The laser beam was scanned over a 50 x 50 μm^2 area on the sample surface and spectra acquired at steps of 1 x 1 μm^2 area. Since the goal is to obtain the distribution of the CNTs in the matrix and CNTs show a very strong G-mode intensity, it becomes more practical to derive the Raman image from the G-mode. It is noted that the distribution of CNT diameters and the distribution of defective CNTs for the scanned area can be obtained by mapping the RB- and D- modes, respectively.

Carbon nanotube dispersion at the nanoscale was analyzed using a JEOL JSM-7500 ultra high resolution field emission scanning electron microscope (FE-SEM) [52,58]. FE-SEM was performed on the fractured cross-section of each specimen. The fractured surface was obtained by breaking the specimen after placing it in liquid nitrogen. The fractured surface of each sample was then coated with a 4nm layer of

Pt/Pd (80% Pt, 20% Pd). Scanning electron microscopy was performed at an acceleration voltage of 2.0 kV with a probe current of 0.03 nA and a working distance of 6 mm.

4. Electrical Characterization

The electrical conductivity (AC) of the nanocomposite samples was tested using a Novocontrol Broadband Dielectric Spectrometer. Testing was performed at room temperature (25 °C) with a voltage amplitude of 1.0 V. The electrical conductivity was determined as a function of frequency over the range of 0.01 Hz to 10 MHz. Test specimen were cut with a 2 x 2 cm^2 area and a 3 mm thickness. Conductive silver paint was brush painted on the bottom and top surfaces of each specimen as a 1 cm diameter circle for use as an electrode. Three samples of each CNT type (pristine, oxidized, and fluorinated XD) for each CNT weight fraction were tested. The DC electrical conductivity was estimated as equivalent to the AC electrical conductivity at the lowest frequency of 0.01 Hz.

5. Thermal Characterization

The thermal conductivity of the nanocomposite samples was determined using a Hot Disk^{TM} Thermal Constants Analyzer [9,30]. Two samples with a 2 x 2 cm^2 area and a thickness of about 3 mm were used for each test. Testing is based on the use of a nickel double spiral sensor that is placed in between two specimen and transiently heated. The heat dissipates to the samples being tested at a rate that depends on the

thermal conductivity and diffusivity of the material. This sensor acts as both the heat source and the temperature sensor, since the change in temperature with time can be obtained from the change in electrical resistance. Testing was performed at room temperature (25 °C) and a total of 6 samples (3 tests with 2 samples each) were tested for each CNT type and weight fraction. No surface preparation was required for the samples.

B. Micromechanics Modeling

A micromechanics approach, obtained from Seidel et al. [82,84], was pursued, based on the composite cylinders method [34], in order to model the thermal and electrical conductivity of CNT/epoxy composites with straight, randomly oriented CNTs. The modeling was done at multiple scales (nano and micro scales) as seen in Figure 6 in order to ultimately determine the effective nanocomposite conductivity.

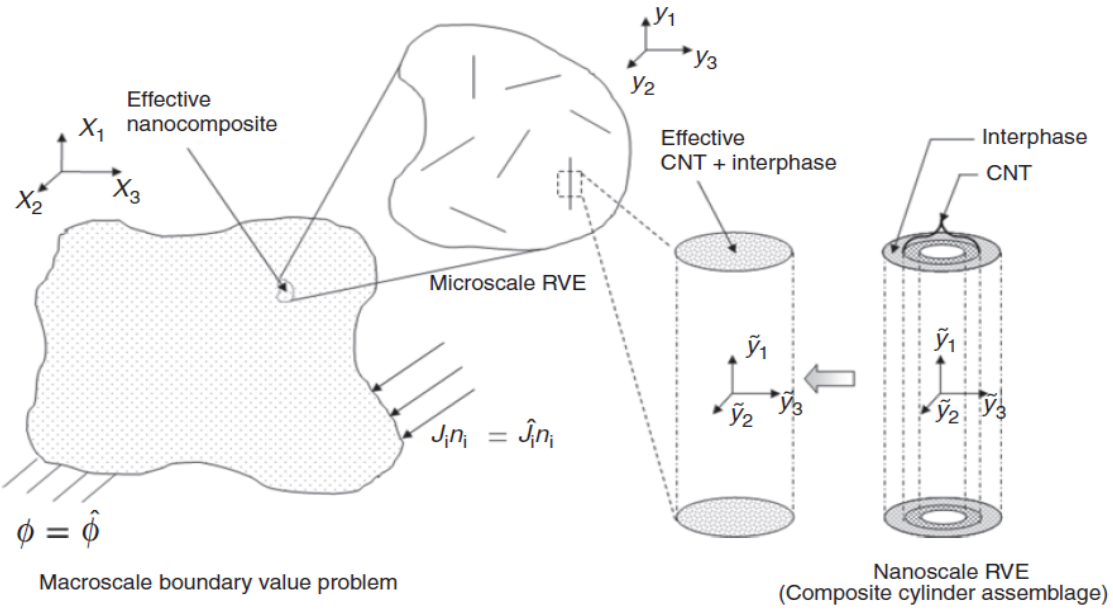

Figure 6. Schematic of the effective CNT/epoxy composite and representative volume elements [82]

A composite cylinder assemblage was used as the representative volume element (RVE) for the CNT and interface at the nanoscale, as shown in Figure 6. This nanoscale RVE was used to obtain the effective conductivity of the CNT/interface.

For the boundary conditions at the macroscale, shown in Figure 6, the electric potential, Φ, was determined from Eq. 1 – 3, where $\mathbf{J}$ is the electric flux vector, $\mathbf{E}$ is the electric field, and $\boldsymbol{\sigma}^{eff}$ is the effective electrical conductivity of the effective nanocomposite. The effective nanocomposite electrical conductivity was determined from the effective electrical conductivity of the microscale RVE, which was obtained from the nanoscale RVE [82], as represented in Figure 6.

$$\nabla \cdot \mathbf{J} = 0 \tag{1}$$

$$\mathbf{J} = \boldsymbol{\sigma}^{eff}\mathbf{E} \tag{2}$$

$$\mathbf{E} = -\nabla \Phi \tag{3}$$

Details on the derivation of all of the following equations are shown in [82,84]. After applying the energy equivalency between the effective homogeneous cylinder and the composite cylinder assemblage, the effective axial and transverse electrical conductivity for the total composite cylinder was obtained as shown in Eq. 4 and 5, respectively, where $\tilde{\sigma}_{11}^{(i)}$ represents the axial electrical conductivity of the *i*th cylindrical layer, $\tilde{\sigma}_{22}^{(i)}$ represents the transverse electrical conductivity of the *i*th cylindrical layer, and the radius of each cylindrical layer is defined in Figure 7. The constants, $D_1^{(i)}$ and $D_2^{(i)}$, in Eq. 5 are obtained from boundary conditions of uniform electrical conduction in the axial and transverse direction, an insulated internal surface, and continuity between cylindrical layers [82].

$$\tilde{\sigma}_{11}^{(effcyl)} = \sum_{i=1}^{N} \tilde{\sigma}_{11}^{(i)} \frac{\left(r_i^2 - r_{i-1}^2\right)}{r_N^2} \tag{4}$$

$$\tilde{\sigma}_{22}^{(effcyl)} = \frac{1}{r_N^2 E_0^2} \sum_{i=1}^{N} \tilde{\sigma}_{22}^{(i)} \left[\left(D_1^{(i)}\right)^2 \left(r_i^2 - r_{i-1}^2\right) - \left(D_2^{(i)}\right)^2 \left(\frac{1}{r_i^2} - \frac{1}{r_{i-1}^2}\right) \right] \tag{5}$$

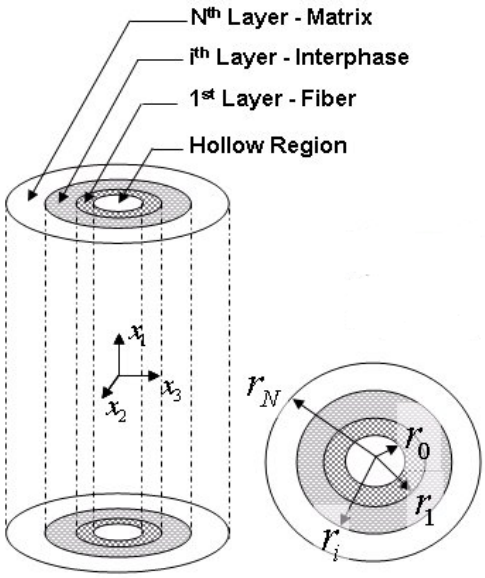

Figure 7. Schematic of layered composite cylinder assemblage [84]

When considering the electron hopping conduction mechanism, the above model for the axial and transverse conductivity can only account for electron hopping in the transverse direction and not for electron hopping through the CNT ends. Therefore, an effective axial conductivity with end effects was obtained from Eq. 6, where σ_{CNT} is the conductivity of the CNT, σ_{int} is the conductivity of the interface layer, l_{CNT} is the length of the CNT, and t_{int} is the thickness of the interface layer. As seen in Figure 8, an interface was added with the same conductivity and thickness as the electron tunneling interface layer in the transverse direction.

$$\tilde{\sigma}_{11}^{(ea)} = \frac{\sigma_{CNT}\sigma_{int}l_{CNT}}{\sigma_{CNT}2t_{int}+\sigma_{int}(l_{CNT}-2t_{int})} \tag{6}$$

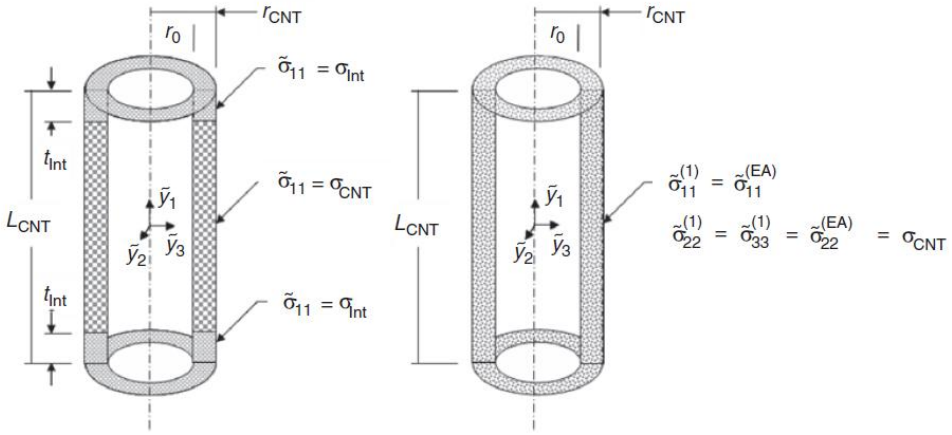

Figure 8. Schematic of CNT with end effects [82]

Therefore, when considering electron hopping (N=3 assemblage, where N is the number of layered cylinders), the conductivites of each layer are as shown in Eq. 7 – 9, where $\tilde{\boldsymbol{\sigma}}^{(1)}$ is the CNT layer, is $\tilde{\boldsymbol{\sigma}}^{(2)}$ the interface layer, and $\tilde{\boldsymbol{\sigma}}^{(3)}$ is the matrix layer.

$$\left[\tilde{\boldsymbol{\sigma}}^{(1)}\right] = \begin{bmatrix} \tilde{\sigma}_{11}^{(ea)} & 0 & 0 \\ 0 & \sigma_{CNT} & 0 \\ 0 & 0 & \sigma_{CNT} \end{bmatrix} \tag{7}$$

$$\left[\tilde{\boldsymbol{\sigma}}^{(2)}\right] = \begin{bmatrix} \sigma_{int} & 0 & 0 \\ 0 & \sigma_{int} & 0 \\ 0 & 0 & \sigma_{int} \end{bmatrix} \tag{8}$$

$$\left[\tilde{\boldsymbol{\sigma}}^{(3)}\right] = \begin{bmatrix} \sigma_{mat} & 0 & 0 \\ 0 & \sigma_{mat} & 0 \\ 0 & 0 & \sigma_{mat} \end{bmatrix} \tag{9}$$

Else if electron hopping is not considered (N=2), then the conductivities are as shown in Eq. 10 and 11, where $\tilde{\boldsymbol{\sigma}}^{(1)}$ is the CNT layer and $\tilde{\boldsymbol{\sigma}}^{(2)}$ becomes the matrix layer.

$$\left[\tilde{\boldsymbol{\sigma}}^{(1)}\right] = \begin{bmatrix} \sigma_{CNT} & 0 & 0 \\ 0 & \sigma_{CNT} & 0 \\ 0 & 0 & \sigma_{CNT} \end{bmatrix} \tag{10}$$

$$\left[\tilde{\boldsymbol{\sigma}}^{(2)}\right] = \begin{bmatrix} \sigma_{mat} & 0 & 0 \\ 0 & \sigma_{mat} & 0 \\ 0 & 0 & \sigma_{mat} \end{bmatrix} \tag{11}$$

Eq. 7 - 9 were then used as input in Eq. 4 and 5 in order to obtain the effective axial and transverse conductivity of the N=3 composite cylinder assemblage. For the N=2 assemblage, Eq. 10 and 11 were used as input.

Once the effective conductivities of the nanoscale RVE were obtained, the effective conductivity of the nanocomposite was obtained from Eq. 12, using the microscale RVE.

$$\boldsymbol{\sigma}^{eff} = \boldsymbol{\sigma}^{(mat)} + \frac{1}{4\pi}\int_0^{2\pi}\int_0^{\pi}\left\{v_f\left(\boldsymbol{\sigma}^{(effcyl)} - \boldsymbol{\sigma}^{(mat)}\right)\boldsymbol{A}\right\}\sin\varphi d\varphi d\psi \tag{12}$$

The conductivity in the local coordinate system, $\tilde{y}_i$, was transformed to the global coordinate system, y_i , by Eq. 13 where Q, Eq. 14, is the direction cosine matrix for the 2-1-3 Euler angles (ψ, ω, φ), where the rotation in the 1-direction is set to zero.

$$\sigma_{ij}^{(effcyl)} = Q_{im}\tilde{\sigma}_{mn}^{(effcyl)}Q_{jn} \tag{13}$$

$$[\boldsymbol{Q}] = \begin{bmatrix} \cos\psi\sin\varphi & \sin\psi\sin\varphi & \cos\varphi \\ -\sin\psi & \cos\psi & 0 \\ -\cos\psi\cos\varphi & -\sin\psi\cos\varphi & \sin\varphi \end{bmatrix} \tag{14}$$

The tensor $\boldsymbol{A}$ in Eq. 12 corresponds to the electric field concentration tensor which relates the average electric field in the nanocomposite to the average electric field in the effective CNT composite cylinder assemblage [82]. Using the Mori-Tanaka method [69,84], the concentration tensor was obtained from Eq. 15 and 16.

$$A_{ij} = Q_{im}\tilde{T}_{mn}Q_{ln}\left\{(1-v_f)\delta_{jl} + \frac{v_f}{4\pi}\int_0^{2\pi}\int_0^{\pi}\{Q_{lr}\tilde{T}_{rs}Q_{js}\}\sin\varphi d\varphi d\psi\right\}^{-1} \tag{15}$$

$$\tilde{T}_{ij} = \left\{\delta_{ji} + S_{jm}\left(\sigma_{nm}^{(mat)}\right)^{-1}\left(\tilde{\sigma}_{ni}^{(effcyl)} - \sigma_{ni}^{(mat)}\right)\right\}^{-1} \tag{16}$$

where v_f is the CNT volume fraction, δ_{ij} is the Kronecker delta and S_{ij} corresponds to the electrical equivalent of the Eshelby tensor [69,71,82,84] and expressed as Eq. 17.

$$[\boldsymbol{S}] = \begin{bmatrix} 1-2L & 0 & 0 \\ 0 & L & 0 \\ 0 & 0 & L \end{bmatrix} \tag{17}$$

where L is equivalent to

$$L = \frac{p^2}{2(p^2-1)} - \frac{p}{2(p^2-1)^{\frac{3}{2}}}\cosh^{-1} p \tag{18}$$

and *p* represents the aspect ratio of the CNT as shown in Eq. 19, where l_{CNT} is the length of the CNT and d_{CNT} is the diameter of the CNT.

$$p = \frac{l_{CNT}}{d_{CNT}} \tag{19}$$

Since the equations for the thermal conductivity are mathematically identical to those for electrical conductivity [84], the same method and equations were used in the micromechanics model for thermal conductivity, with σ being replaced with k.

In order to account for the nanoscale effects present in both the thermal and electrical conductivity of CNTs, interface regions were introduced to include phonon scattering and electron tunneling. The scattering of phonons present in the thermal conduction of CNT/epoxy composites was accounted for by an interfacial thermal

resistance layer, or Kapitza resistance [12,71], between the CNT and the matrix. The value of resistance in this layer reflects the magnitude of phonon scattering caused by the presence of the interface and scattering as a result of the presence of defects in the CNT. Electron tunneling was considered by introducing an electrically conductive interface layer, between the CNT and matrix, with a magnitude greater than that of the matrix but less than the CNT. As volume fraction increases, a CNT is brought into closer proximity to another CNT and there is an increase in the probability of having electron hopping from CNT to CNT. Therefore, the magnitude of the interface layer reflects the increase in electrical conductivity in the composite cylinder assemblage due to the likelihood of the electron tunneling conduction mechanism.

CHAPTER III

RESULTS AND DISCUSSION

This chapter focuses on presenting both experimental and theoretical results obtained from the characterization of XD CNT/epoxy composites. The characterization of pristine, oxidized, and fluorinated XD CNT bundles is presented. The dispersion of the CNTs in the epoxy matrix is examined along with electrical and thermal conductivity results for each fabricated sample type. Finally, the micromechanics modeling results are shown and the agreement with experimental results discussed.

A. Characterization of XD CNTs

Raman spectroscopy performed on each XD CNT type is shown in Figure 9. As stated before, the D-band measures the disorder, or the breaking of symmetry, created by the presence of defects or by functionalization of a CNT. As seen in Figure 9, the intensity of the D-band is high for oxidized XD CNTs, relative to pristine XD CNTs, and even higher for fluorinated XD CNTs. This result suggests that functionalization of XD CNTs might create significant damage to the CNT wall and also introduce asymmetry to the crystalline structure.

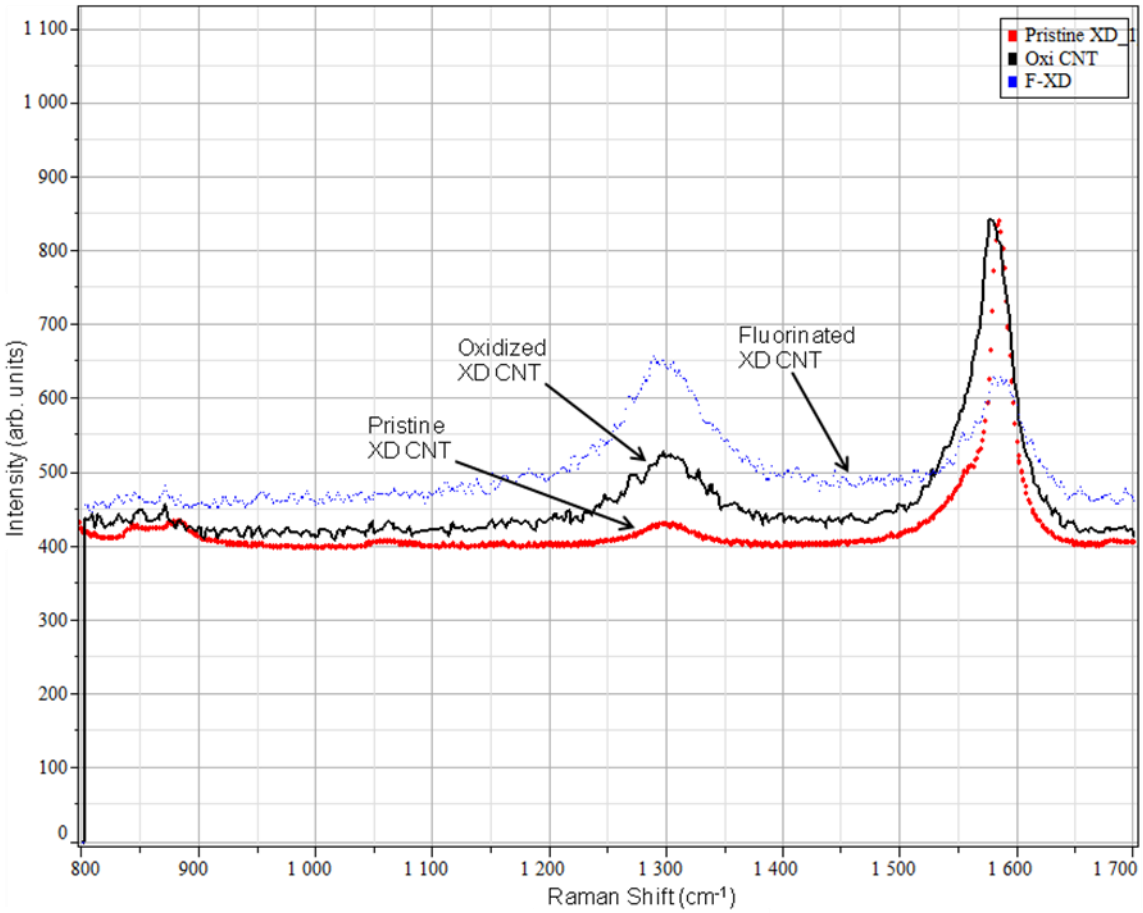

Figure 9. Raman spectra of pristine, oxidized, and fluorinated XD CNTs

SEM images of the resulting ball-milled XD CNT bundles are shown in Figure 10 for varying ball-milling time.

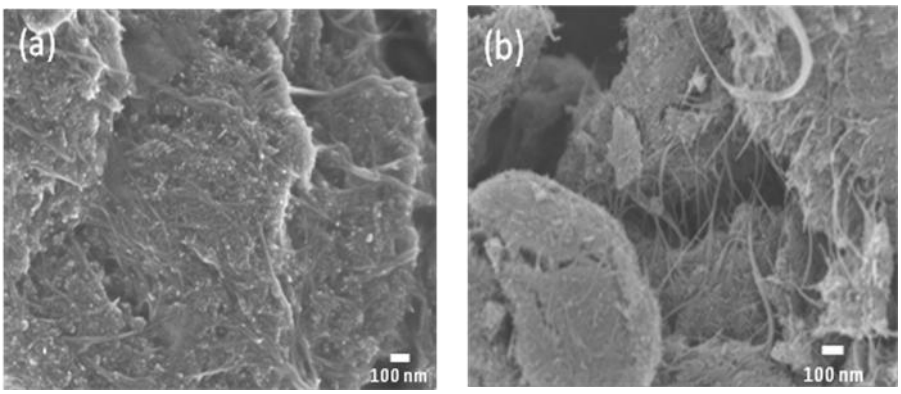

Figure 10. SEM image of ball milled pristine XD CNT bundles (a) 5 minutes (b) 10 minutes

As seen in Figure 10, pristine XD CNT bundles tend to compact when ball-milled. One important result of the ball-milling of XD CNTs is that the aggregates present in the supplied pristine XD CNTs, as seen in Figure 11a, are reduced in size. The ball-milled XD CNT bundles also show less entanglement than non-milled XD CNT bundles as seen in Figure 11b.

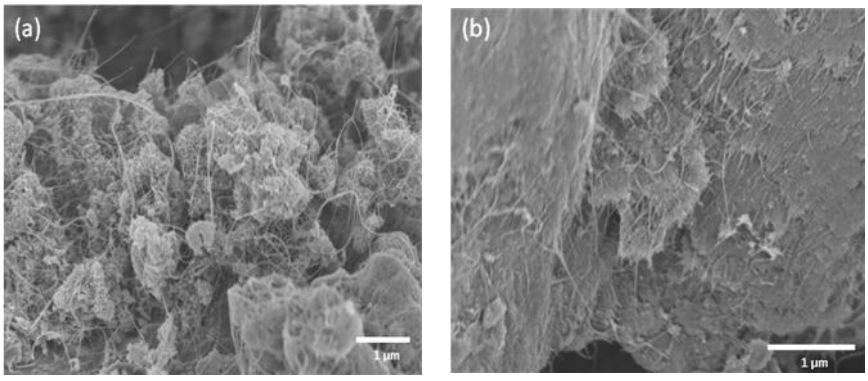

Figure 11. Ball milled XD CNT bundles (a) 0 min (as received) (b) 10 min

Raman spectra of the ball-milled XD CNT bundles at different ball-milling times is shown in Figure 12.

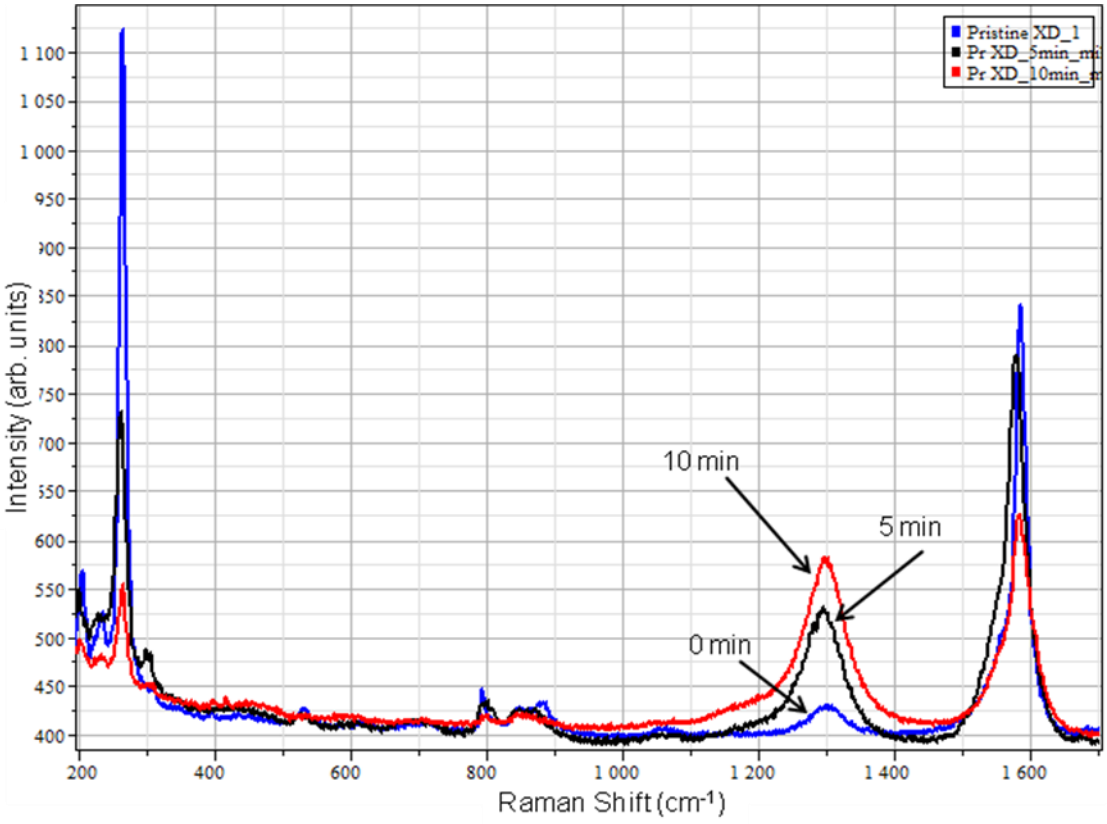

Figure 12. Raman spectra of pristine XD CNTs at different ball milling times

As stated previously, the D-band, between 1290-1360 cm^{-1}, is a measure of the disorder in the CNT and it is activated by the presence of defects or the breaking of symmetry in the CNT structure [112]. According to Li et al., when ball-milling CNTs, the high velocity and frequent collision of the steel balls with the CNTs can damage the nanotube cylindrical structure if the impact is high enough [55]. In Figure 12, the

intensity of the D-band increases with ball-milling time, suggesting defects are introduced into the CNT structure. The longer the ball-milling time, the more defects created on the structure.

B. Dispersion Analysis of XD CNT/Epoxy Composites

One of the most important requirements for improving the properties of epoxy by the use of nanoinclusions is obtaining a homogeneous dispersion of the nanofiller. Carbon nanotubes tend to form large agglomerates due to intermolecular Van der Waals forces [113]. Obtaining nanocomposites with a high degree of dispersion is desired in order to obtain improved thermal and electrical conductivity of the composite [94]. The analysis of the dispersion of CNTs in a nanocomposite will vary depending on the magnification at which the analysis is performed. In order to make a distinction between dispersion at different scales, the definition by Li et al. for the dispersion of CNTs will be used [54]. According to Li et al., "dispersion in CNT/polymer composites has two aspects: i) disentanglement of CNT bundles or agglomerates, which is a nanoscopic dispersion, and ii) uniform distribution of individual CNTs or their agglomerates throughout the nanocomposites, which is more of a micro- and macroscopic dispersion" [54]. Therefore, the Optical Microscopy and Raman Imaging results will analyze the uniformity of the agglomerate and CNT distribution, while SEM results will show if the CNTs are disentangled. The dispersion of CNTs is qualitatively described at the length scale of observation.

As seen in Figure 13, the baseline fabrication procedure mentioned earlier results in poor CNT dispersion with pristine XD CNTs, evident in the formation and non-uniform distribution of large agglomerates. In order to determine if the mold orientation during curing contributes to agglomeration, the XD CNT/epoxy solution was cured both vertically and horizontally. As seen in Figure 13(a), the CNTs experience a gravity effect, the CNTs are sinking to the bottom of the mold resulting in large agglomerates when cured in the vertical position. When cured in the horizontal position, results indicate that there is a more uniform distribution of the CNT agglomerates, but there is still movement of CNTs as seen in Figure 13(b).

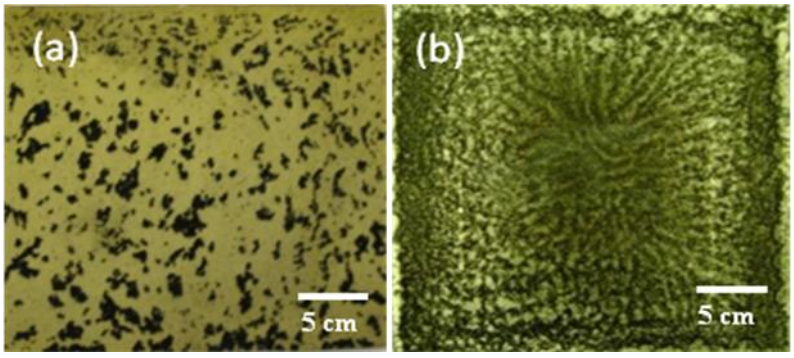

Figure 13. 0.015wt% pristine XD/epoxy composite cured in (a) vertical (b) horizontal position

The sinking of the CNTs suggests that there is movement of the CNTs during curing, possibly due to convective heat flow [65]. Also, the decrease in viscosity at the higher temperature of 122 °C allows and facilitates the movement of CNTs, resulting in severe agglomeration. In order to improve the dispersion of XD CNTs in the epoxy

matrix, focus was shifted to modifying the baseline procedure by controlling two main parameters- rate of stirring and the viscosity of the epoxy prior to curing. An increase in the rate of stirring would result in higher shearing forces in the resin and should reduce the degree of agglomeration by breaking up the agglomerates, if the shearing force overcomes the Van der Waals attraction between the CNTs. An increase in the viscosity of the epoxy prior to full curing would reduce the movement of CNTs at temperatures above 25 °C.

The stirring rate was increased from 60 rpm to 400 rpm, using the same fabrication procedure mentioned earlier. The resulting CNT distribution is shown in Figure 14. The composite shows improvement in CNT agglomerate distribution, as evident in the decrease of agglomerate size, and more uniform distribution at the center, even though the overall distribution of CNTs is still poor.

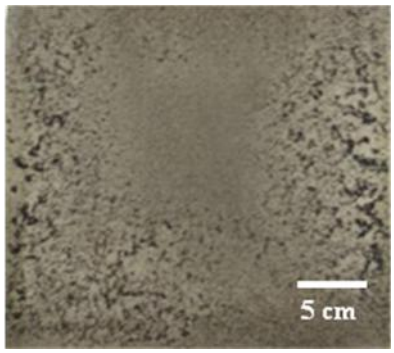

Figure 14. 0.015wt% pristine XD/epoxy composite with stirring at 400 rpm

Even though the size of agglomerates in the cured samples was reduced by increasing the stirring rate, resin and CNT movement during curing, due to reduced

viscosity, increased the size of the agglomerates and resulted in a non-uniform, heterogeneous distribution of CNTs. Thus, if the XD CNT/epoxy viscosity were to be increased prior to fully curing the epoxy, an improvement in CNT dispersion should result by reducing the movement of CNTs. By partially curing the epoxy before pouring it in the mold, using the procedure outlined previously, not only is the viscosity increased but the effectiveness of the shear stirring is enhanced. The dispersion of pristine XD CNTs for different pre-curing times is seen in Figure 15.

The micrographs show a gradual improvement in CNT agglomerate distribution and a decrease in agglomerate size with increasing pre-curing time. The results suggest that the higher the viscosity of the epoxy, the more the improvement in CNT agglomerate distribution. The pre-curing technique also shows a more uniform distribution of agglomerate size.

The distribution of CNT agglomerates in epoxy is shown in Figure 16-18 for pristine, oxidized, and fluorinated XD CNTs at different XD CNT weight fractions, stirred at 400 rpm and pre-cured for 200 minutes.

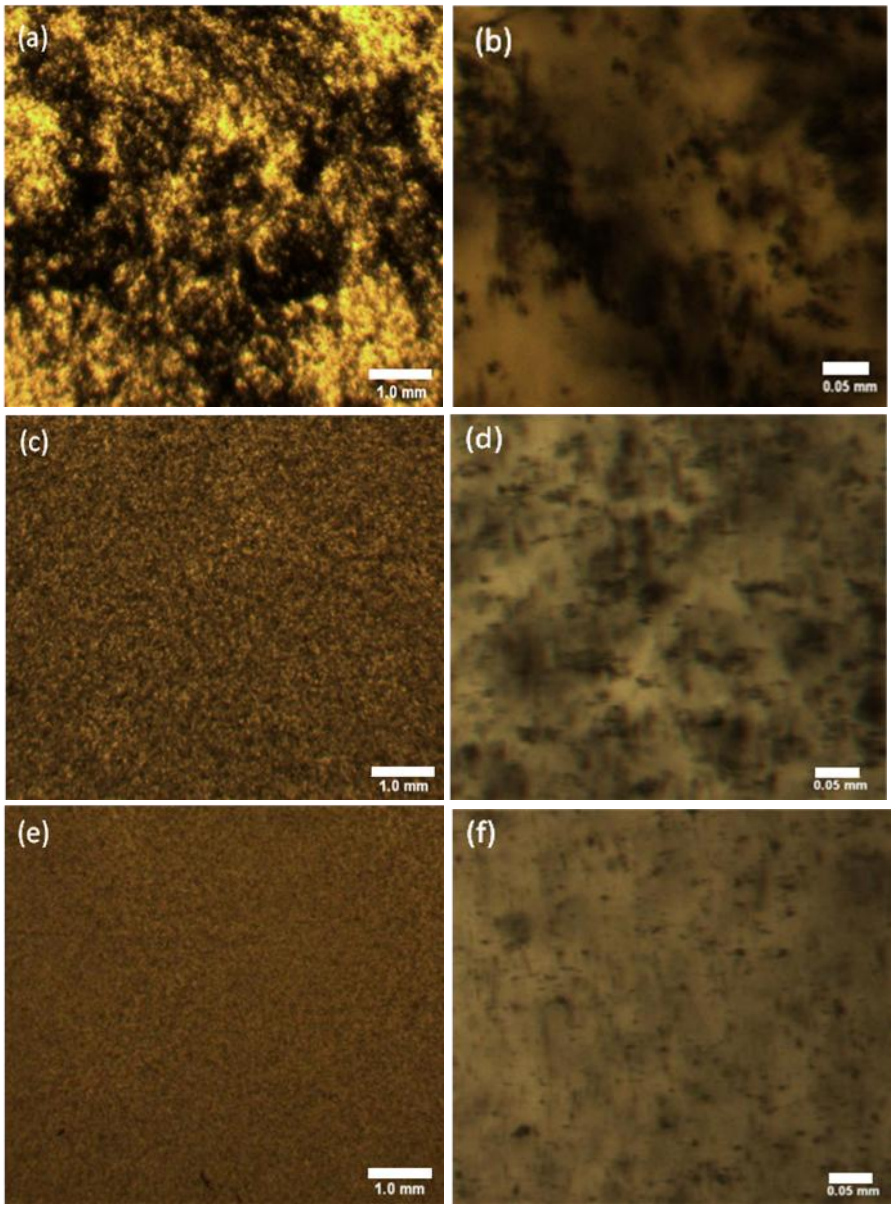

Figure 15. OM images showing the affect of pre-curing time for 0.015wt% pristine XD CNT composite (a) 0 minutes 25X (b) 0 minutes 400X (c) 180min 25X (d) 180 min 400X (e) 200 min 25X (f) 200 min 400X

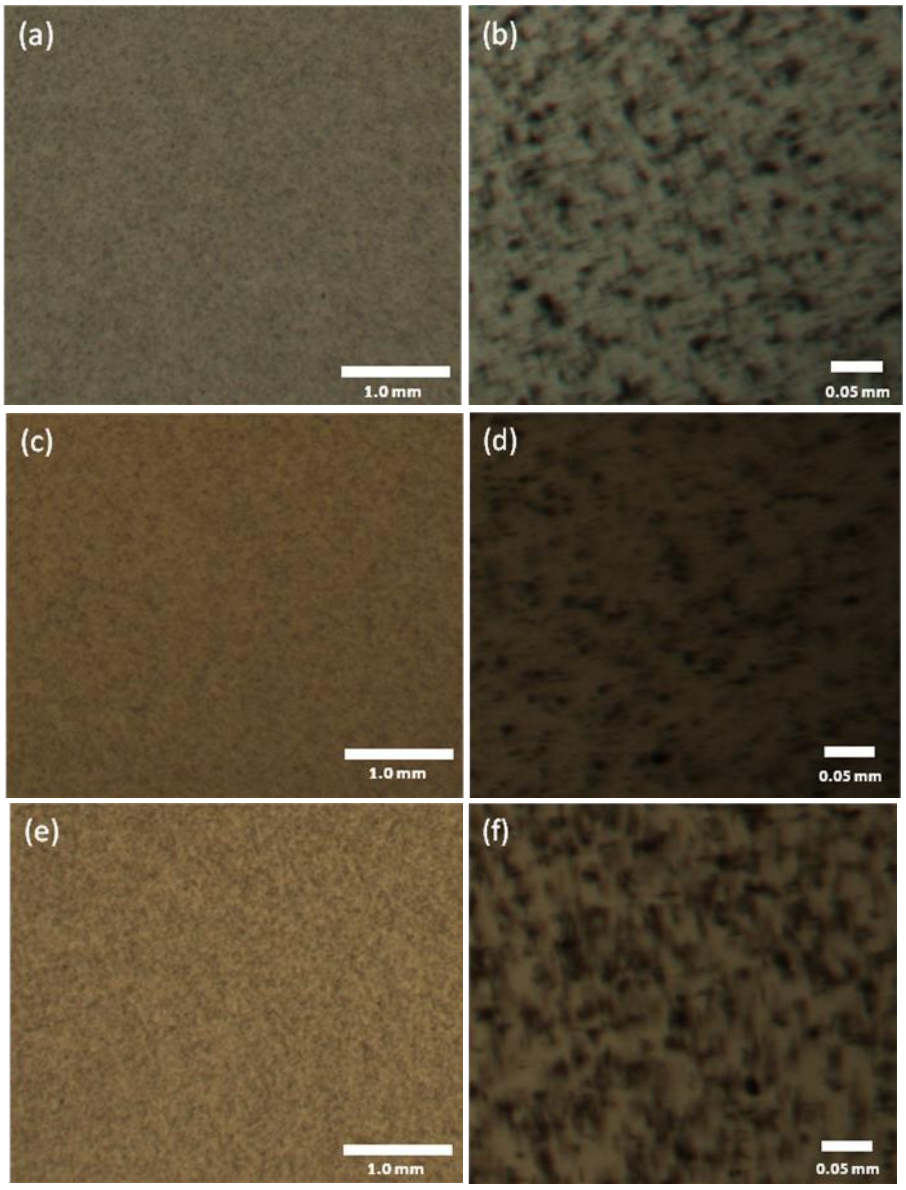

Figure 16. OM images of composites with 0.05wt% (a) pristine XD CNT 25X (b) pristine XD CNT 400X (c) oxidized XD CNT 25X (d) oxidized XD CNT 400X (e) fluorinated XD CNT 25X (f) fluorinated XD CNT 400X

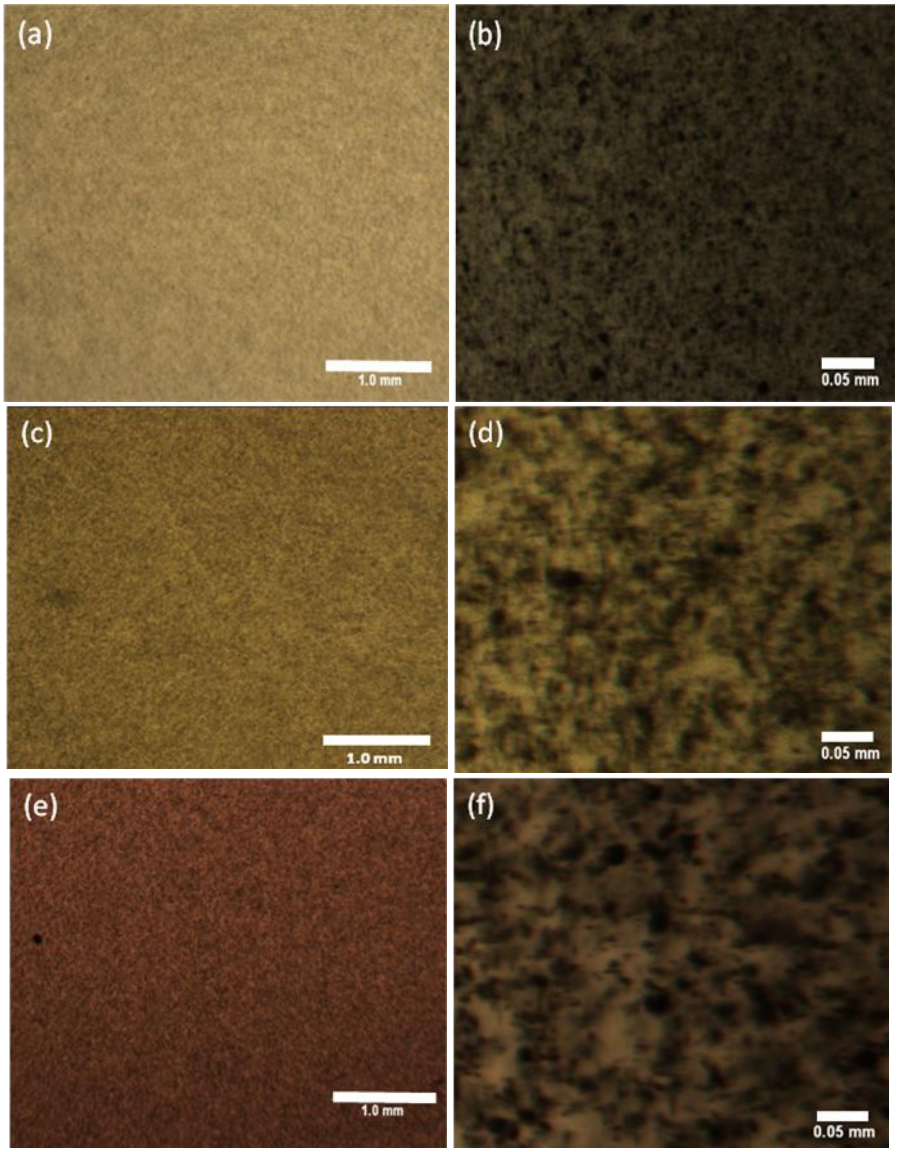

Figure 17. OM images of composites with 0.1wt% (a) pristine XD CNT 25X (b) pristine XD CNT 400X (c) oxidized XD CNT 25X (d) oxidized XD CNT 400X (e) fluorinated XD CNT 25X (f) fluorinated XD CNT 400X

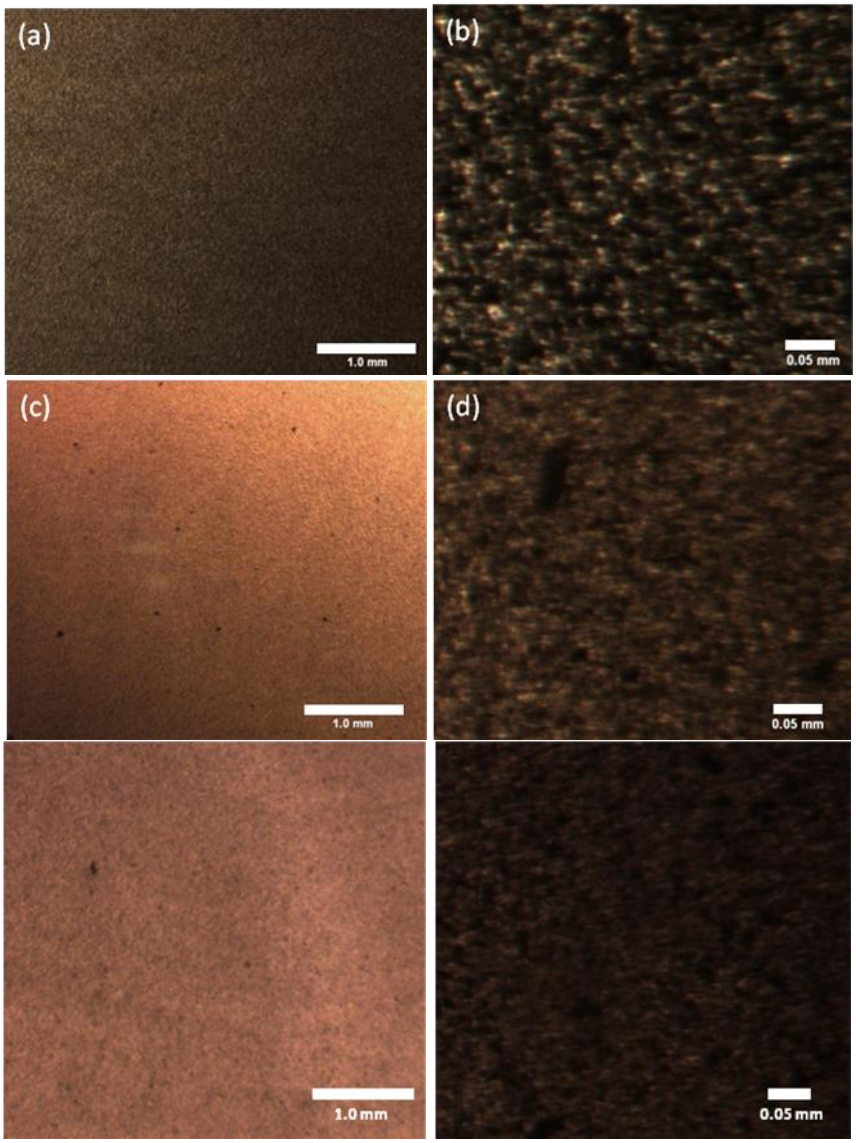

Figure 18. OM images of composites with 0.6wt% (a) pristine XD CNT 25X (b) pristine XD CNT 400X (c) oxidized XD CNT 25X (d) oxidized XD CNT 400X (e) fluorinated XD CNT 25X (f) fluorinated XD CNT 400X

As expected, the nanocomposite becomes more opaque with increasing weight fraction. At the macroscale, the distribution of the CNT agglomerates remains uniform as weight fraction is increased, although the size of the CNT agglomerates shows a slight increase with CNT weight fraction. The size of the agglomerates for the oxidized XD CNT case is slightly smaller in diameter than that for the pristine XD CNT case, specifically at the higher CNT weight fraction of 0.6wt%. The use of fluorinated XD CNTs maintains the uniformity of the distribution of CNT agglomerates. Surprisingly, the dispersion of the pristine XD CNTs in the epoxy is very similar to that of the chemically treated XD CNTs. The results at this scale indicate that oxide and fluorine functionalization is not significantly helpful for improving the dispersion of CNTs in epoxy, for this processing method.

Raman imaging was performed in order to analyze the dispersion of CNT at the microscale. As seen in Figure 19, the distribution of CNTs seems less uniform at low CNT weight fractions. As weight fraction increases, the uniformity of the CNT agglomerate distribution increases, as seen in Figure 20. The agglomerate diameter size observed in the optical micrographs is confirmed by Raman imaging, with an agglomerate diameter ranging from 5-10 μm for pristine, oxidized, and fluorinated XD CNTs. Oxidized XD CNT/epoxy samples show slightly improved uniformity of agglomerates, relative to pristine and fluorinated XD CNTs in Figure 20, however the dispersion remains similar.

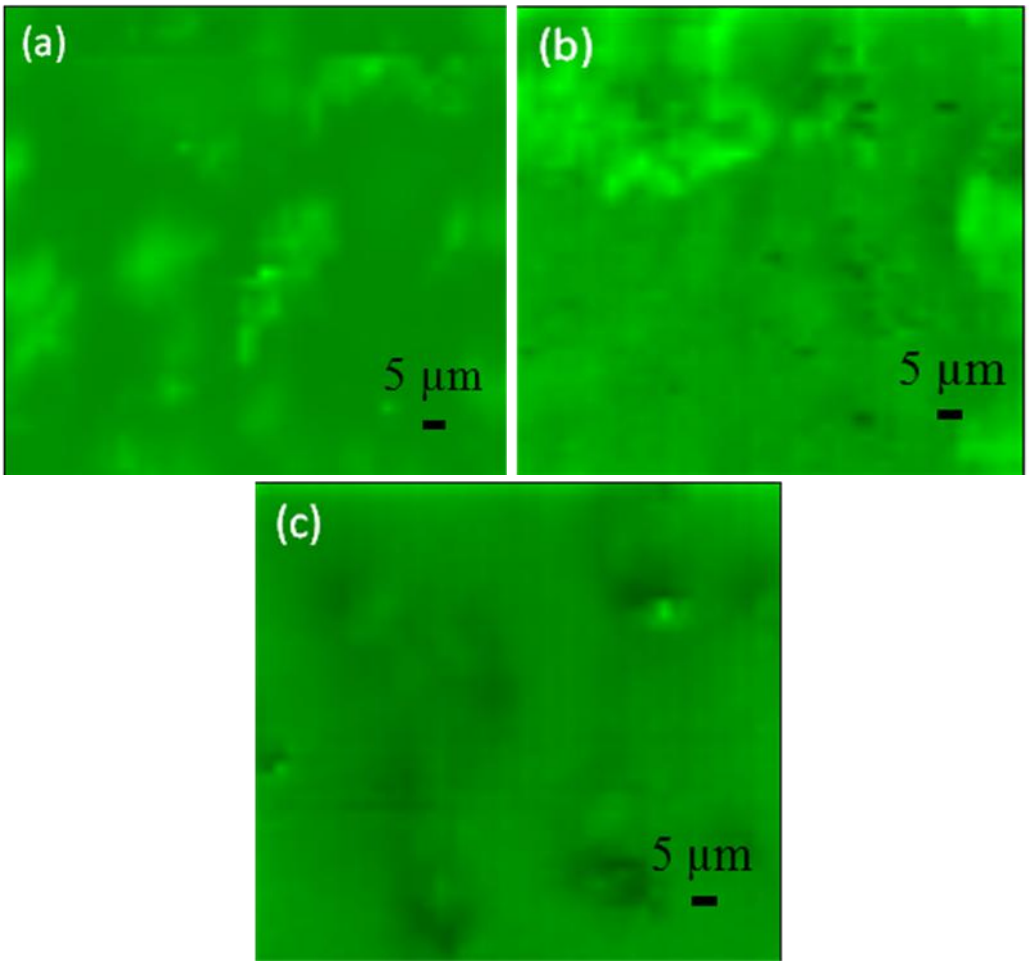

Figure 19. Raman image of composite with 0.05wt% (a) pristine XD CNT (b) oxidized XD CNT (c) fluorinated XD CNT (Brighter color corresponds to higher G-band intensity)

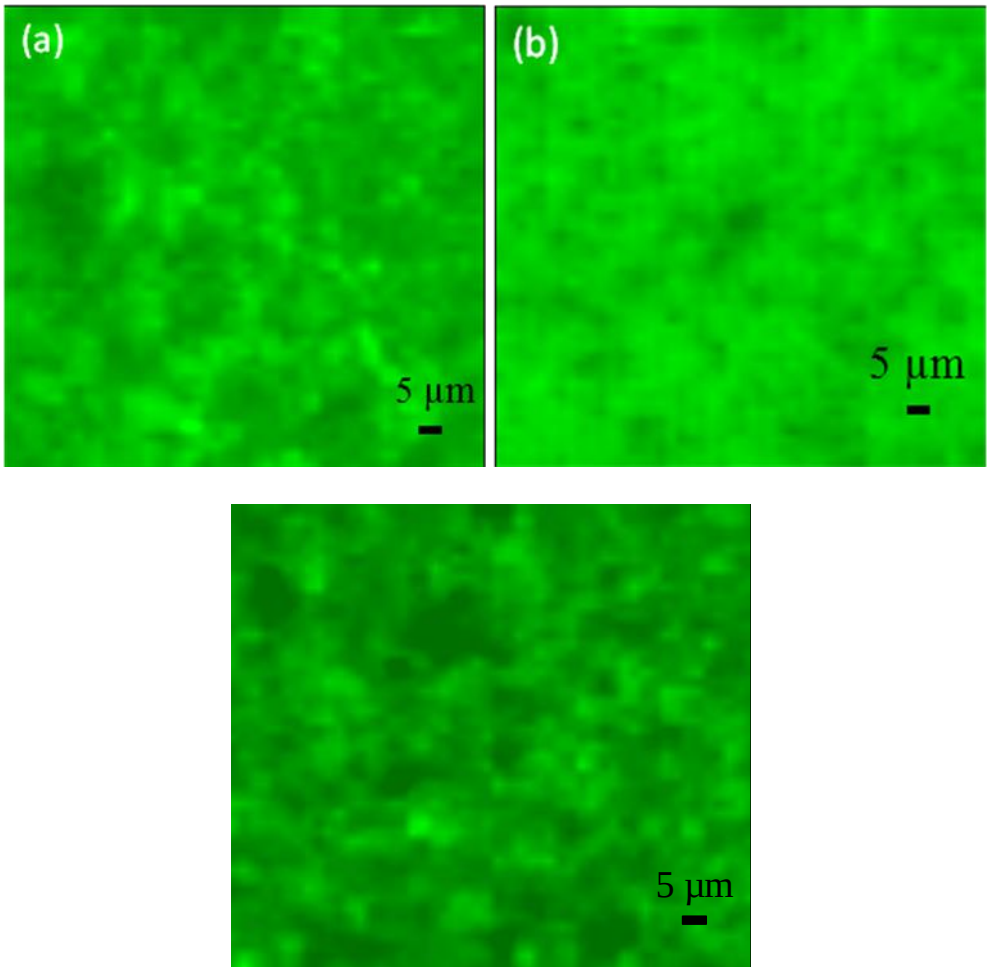

Figure 20. Raman image of composite with 0.6wt% (a) pristine XD CNT (b) oxidized XD CNT (c) fluorinated XD CNT (Brighter color corresponds to higher G-band intensity)

Ball milling the XD CNT bundles results in improved distribution and reduction in size of agglomerates. As seen in Figure 21-22, the diameter of the agglomerates is smaller, $\leq$ 5 µm, than with non-milled CNTs at the same weight fraction. Also, the distribution of ball-milled CNTs is more uniform than with non-milled CNTs. Also, the diameter of the agglomerates decreases with ball-milling time. As observed in the non-

milled samples, the diameter of the ball-milled XD CNT agglomerates also increases with CNT weight fraction.

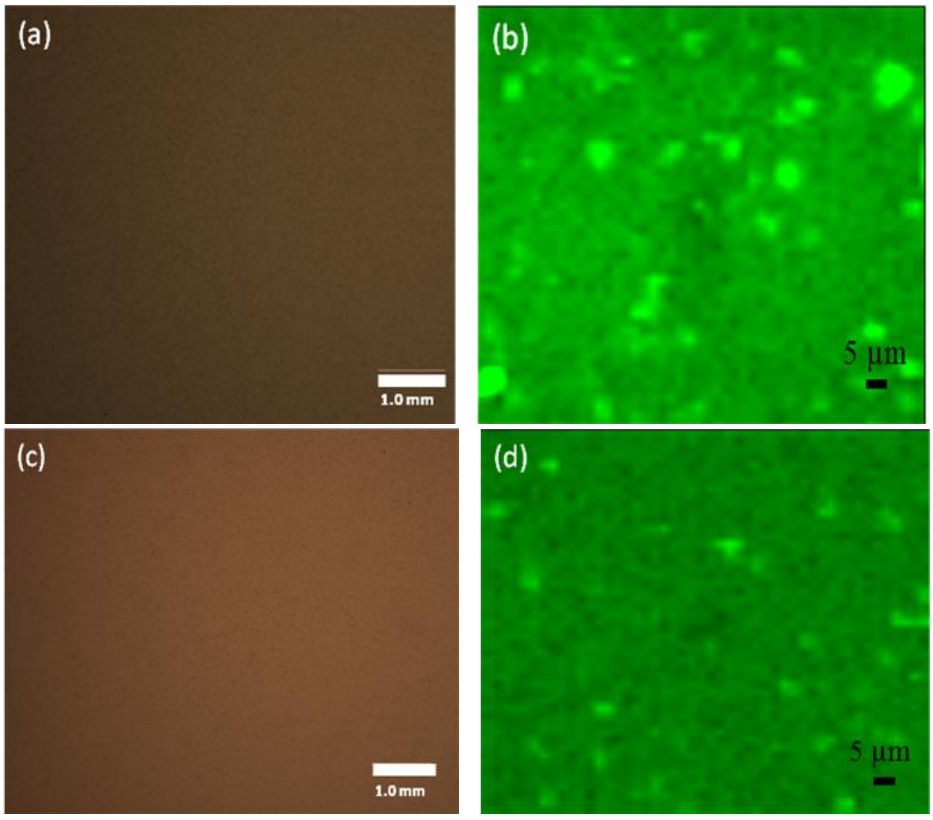

Figure 21. (a) OM image (b) Raman image of 5 minute mill 0.1wt % pristine XD CNT composite (c) OM image (d) Raman image of 10 minute mill 0.1wt % pristine XD CNT composite (Brighter color corresponds to higher G-band intensity)

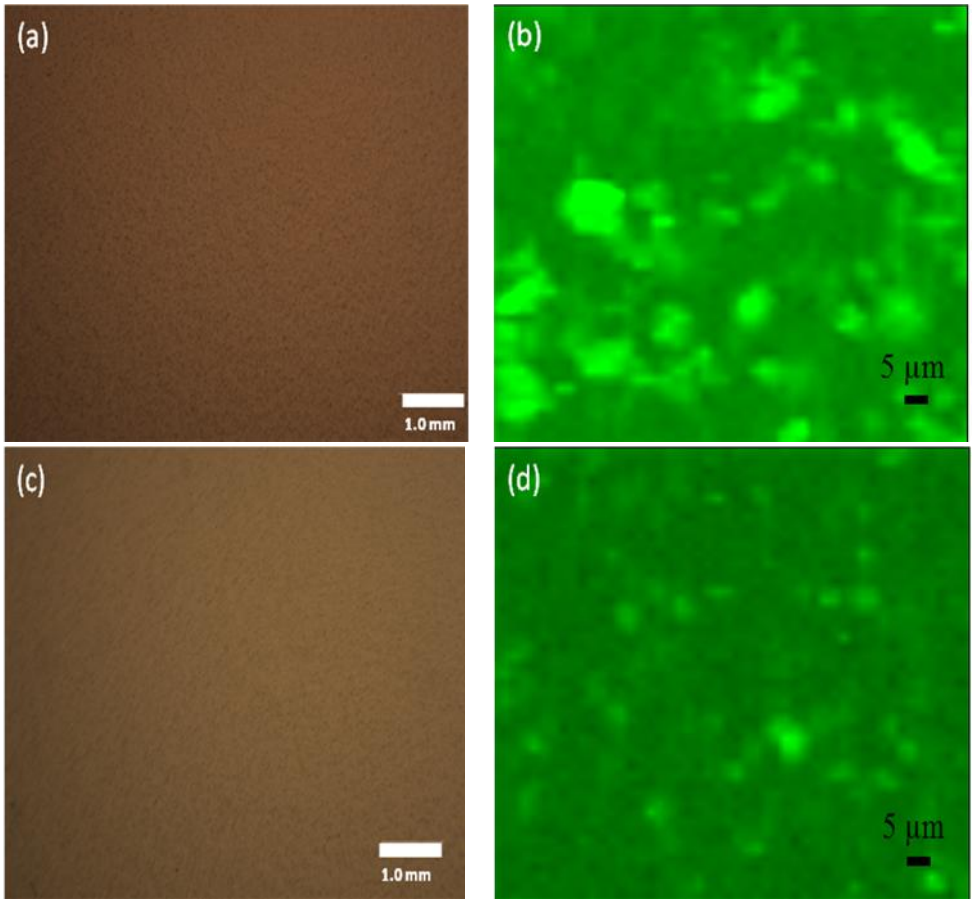

Figure 22. (a) OM image (b) Raman image of 5 minute mill 0.3wt % pristine XD CNT composite (c) OM image (d) Raman image of 10 minute mill 0.3wt % pristine XD CNT composite (Brighter color corresponds to higher G-band intensity)

One reason for the improved dispersion using ball-milled XD CNTs might be the breaking up of the large aggregates present in the supplied XD CNT material, as shown in Figure 11. The ball-milled XD CNTs are less entangled and thus it is easier for individual CNTs to separate and disperse. As shown by [80], using previously aligned, non-entangled CNTs instead of entangled CNTs before mixing with the polymer, to obtain a randomly oriented CNT composite, leads to significant improvement in dispersion.

SEM images in Figure 23 show that XD CNTs in the composite are not individually dispersed but are in agglomerate form. The oxidized XD CNT composites (Figure 23c,d) show less entanglement of CNTs than do both the pristine and fluorinated XD CNT composites, which supports the results seen in the optical micrographs and the Raman images that oxidized XD CNTs provide slightly improved CNT distribution.

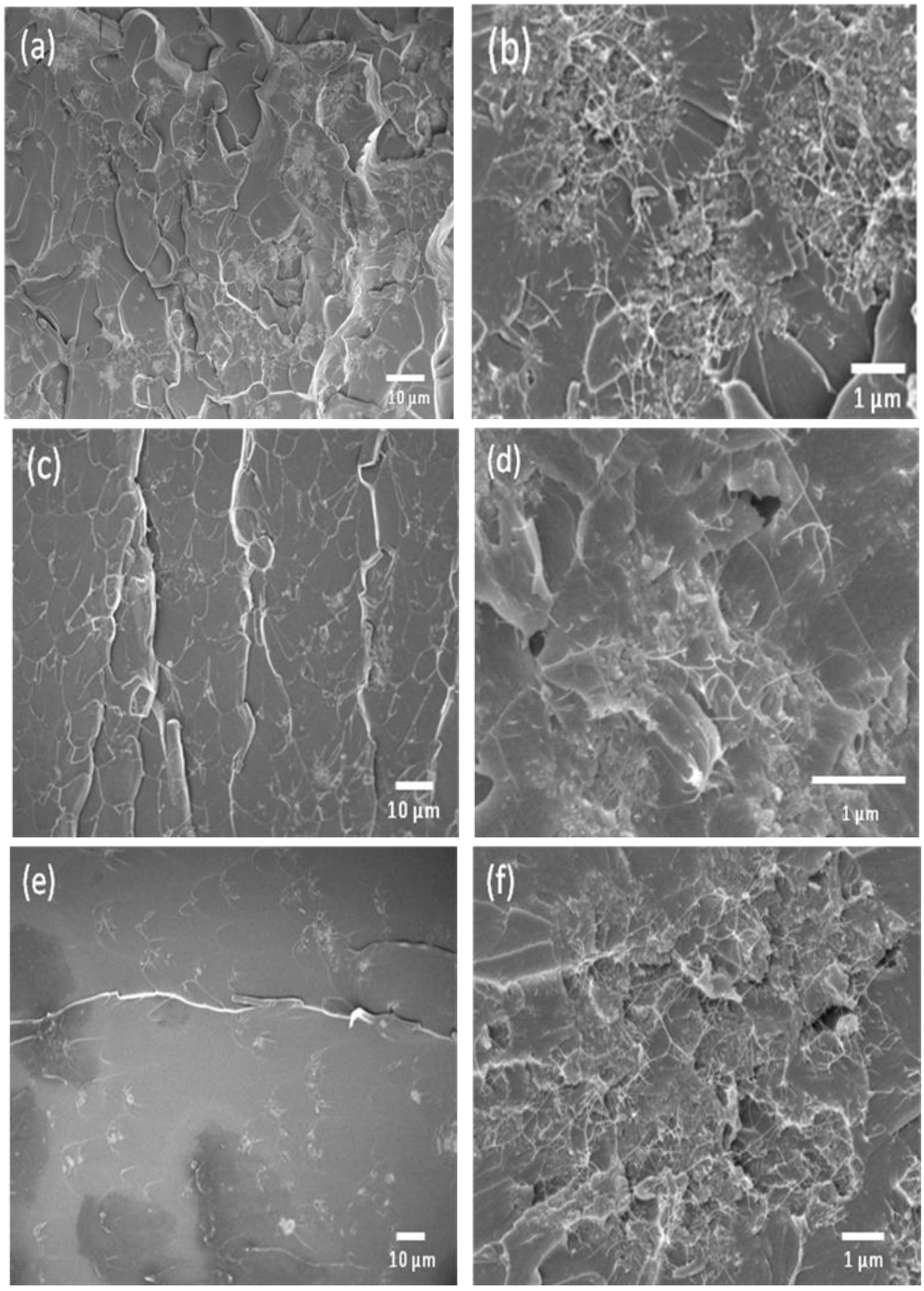

Figure 23. SEM image of composite with 0.3wt% (a,b) pristine XD CNT (c,d) oxidized XD CNT (e,f) fluorinated XD CNT

The SEM results obtained for the ball-milled pristine XD CNT composites are shown in Figure 24. The CNTs in these composites are still somewhat entangled even though smaller agglomerates are present. As seen in Figures 24(a) and 24(c), the agglomerate size decreases with increasing ball-milling time, as also shown by Raman imaging. The agglomerates present in the ball-milled samples seem to be further apart than in the non-ball-milled XD CNT composites.

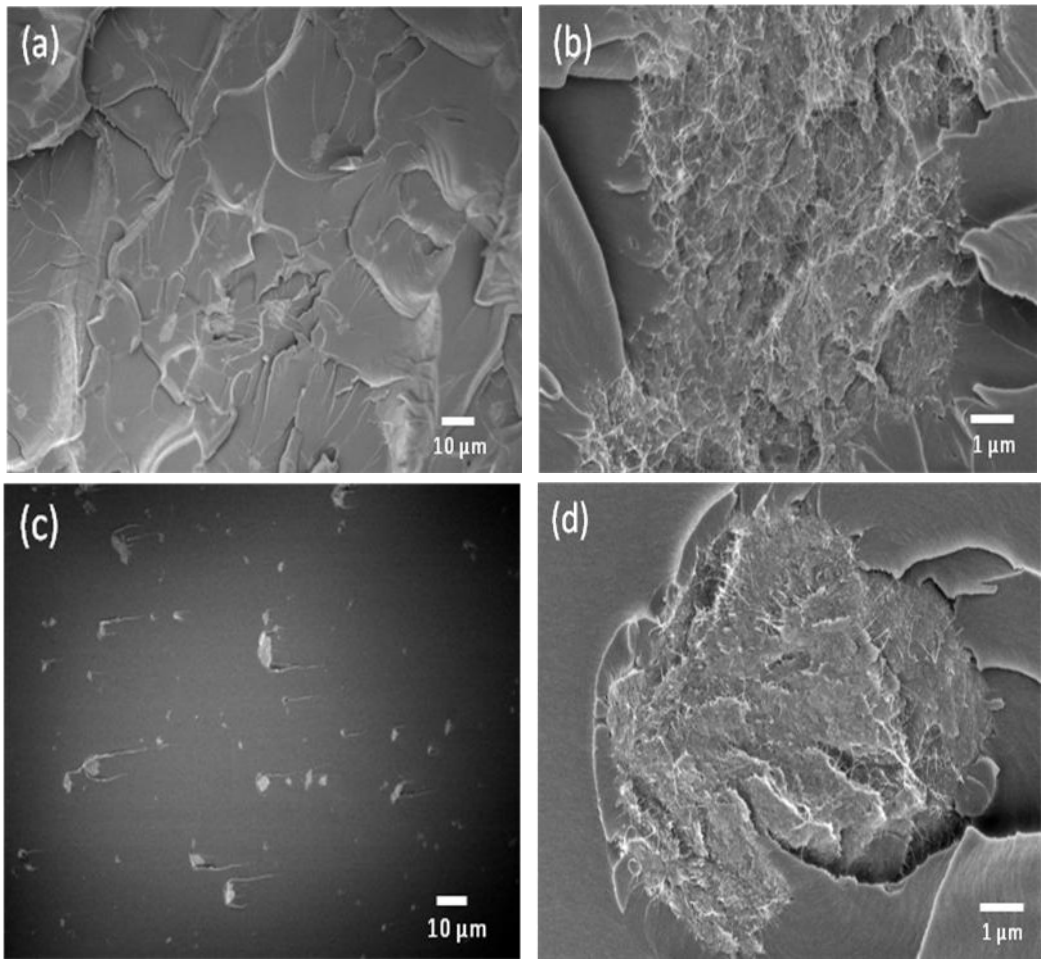

Figure 24. SEM image of composite with pristine 0.3wt% ball-milled for (a,b) 5 min (c,d) 10 min

C. Electrical Conductivity of XD CNT/Epoxy Composites

The AC electrical conductivity as a function of frequency for pristine XD/epoxy composites of different CNT weight fractions is shown in Figure 25.

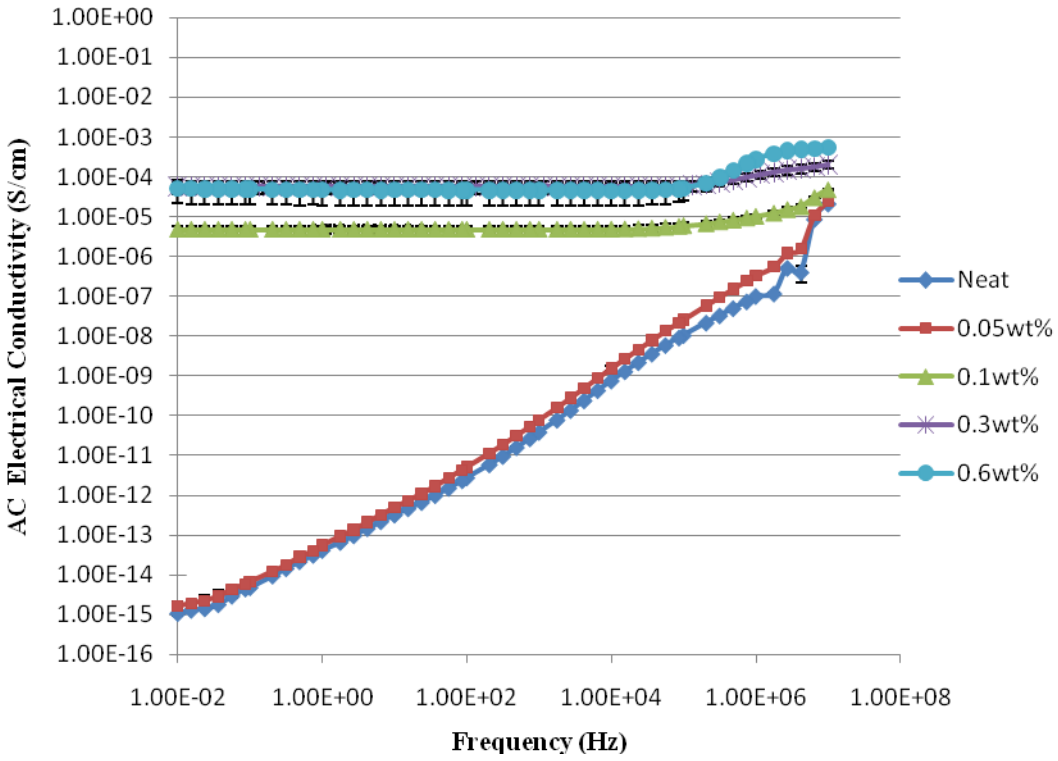

Figure 25. AC electrical conductivity vs. frequency for pristine XD CNT composites as a function of CNT weight fraction

Strong frequency dependence, that is, an increase in AC electrical conductivity with an increase in frequency, is observed for the neat epoxy, which is characteristic of an electrical insulator [4,65,80,95]. An insulating polymer material can become electrically conductive by the addition of electrically conductive inclusions, which will

begin to form conductive paths. The concentration at which a conductive network is formed, known as the percolation threshold, will result in an increase of orders of magnitude in electrical conductivity, as predicted by percolation theory [28,79,106]. The frequency dependent conductivity observed for 0.05wt% pristine XD CNT indicates that these composite samples remain non-conductive, and thus below the percolation threshold. As seen in Figure 25, a significant increase from 1.06E-15 to 4.74E-6 S/cm in electrical conductivity at a frequency of 0.01 Hz is present at a weight fraction of 0.1wt% pristine XD CNT. The increase in electrical conductivity of about 9 orders of magnitude indicates that the percolation threshold is between a pristine XD CNT weight fraction of 0.05 and 0.1wt%; however, there is about one order of magnitude increase from 0.1 to 0.3wt% also at low frequencies. One important observation is that post-percolation, the AC electrical conductivity becomes nearly frequency independent. Once the percolation threshold is reached, minimal increase in electrical conductivity is observed and an electrical conductivity plateau is observed as CNT weight fraction is increased. At low frequencies, the AC electrical conductivity remains constant with increasing frequency up to a characteristic frequency in the high frequency region above which an increase in frequency results in an increase in electrical conductivity. In order to explain this behavior, the AC electrical conductivity of the CNT/epoxy composite is obtained by modeling the complex admittance, Y, as a resistor and capacitor in parallel as defined in Eq. 20 [38,48,72,79,80].

$$Y(\omega) = Y' + Y'' = \frac{1}{R} + j\omega C \tag{20}$$

where R is the resistance, C is the capacitance, and ω is the angular frequency equal to $2\pi f$, where f is the frequency. The AC electrical conductivity, $\sigma_{AC}(\omega)$, is then determined from Eq. 21.

$$\sigma_{AC}(\omega) = |Y(\omega)|\frac{t}{A} \tag{21}$$

where t is the sample thickness, and A is the electrode area. The DC electrical conductivity, σ_{DC}, is then determined from Eq. 22.

$$\sigma_{DC} = Y'\frac{t}{A} \tag{22}$$

The resistor-capacitor model can be used to analyze and explain the results in Figure 25. As seen in Eq. 20 and 21, the ohmic behavior, $\frac{1}{R}$, and the frequency induced dielectric behavior, $j\omega C$, contribute to the total AC electrical conductivity. At CNT weight fractions below the percolation threshold, the influence of Y' is very small due to the lack of conductive pathways, and therefore Y''dominates the AC conductivity. This frequency dependence maintains the composite a dielectric material behaving as a capacitor. Post percolation, the conductivity is dominated by ohmic behavior [79], as a result of charge carriers traveling through the conductive pathways [53], and therefore the real part of the admittance dominates the conductivity, with the effect of frequency only significant at higher frequency values.

The results for the AC electrical conductivity as a function of frequency for oxidized XD/epoxy composites of different CNT weight fractions is shown in Figure 26.

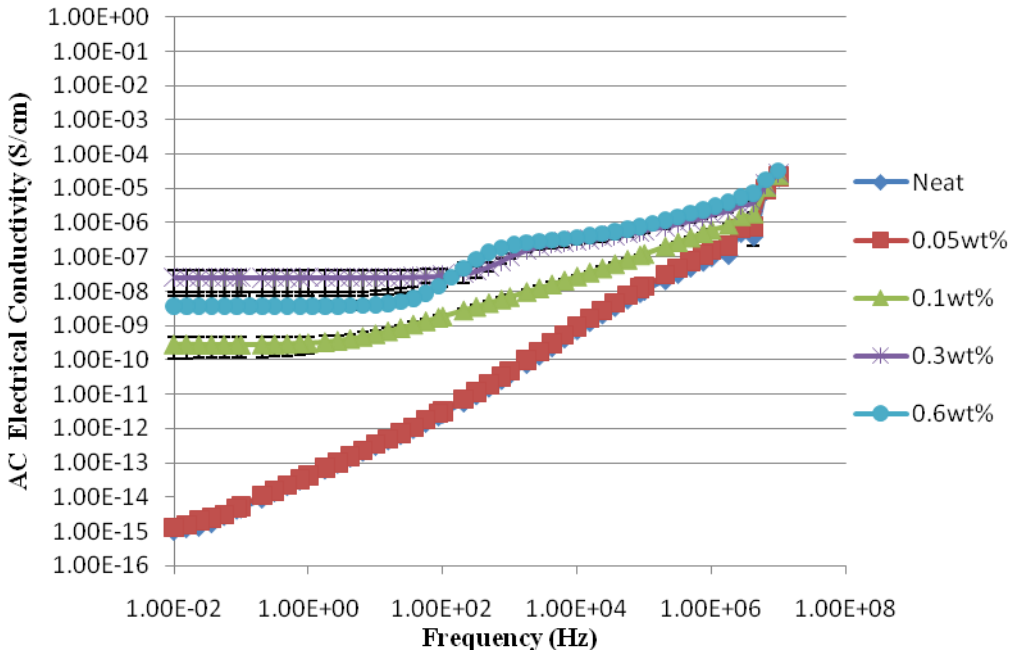

Figure 26. AC electrical conductivity vs. frequency for oxidized XD CNT composites as a function of CNT weight fraction

The same frequency dependence seen for the pristine XD CNT loaded samples below 0.1wt% is also observed in the oxidized XD CNT samples. At 0.05wt% the samples remain non-conductive, but a significant increase in electrical conductivity at a 0.1wt% oxidized XD CNT weight fraction at low frequencies is seen. Thus, the percolation threshold lies between a CNT weight fraction of 0.05 and 0.1wt% oxidized XD CNT. There is an increase in electrical conductivity of about 5 orders of magnitude,

from 1.31E-15 to 2.94E-10 S/cm, for 0.1wt% oxidized XD CNT relative to the neat sample at a low frequency of 0.01 Hz, which corresponds to the DC electrical conductivity. An increase of two orders of magnitude in electrical conductivity results when increasing the weight fraction from 0.1 to 0.3wt%. When compared to the electrical conductivity of pristine XD CNT composites, oxidized XD CNT composites show a decrease of 4 orders of magnitude in electrical conductivity. This decrease in electrical conductivity is observed for all oxidized CNT weight fractions post-percolation.

The AC electrical conductivity as a function of frequency for the fluorinated XD/epoxy composites of different CNT weight fractions is shown in Figure 27.

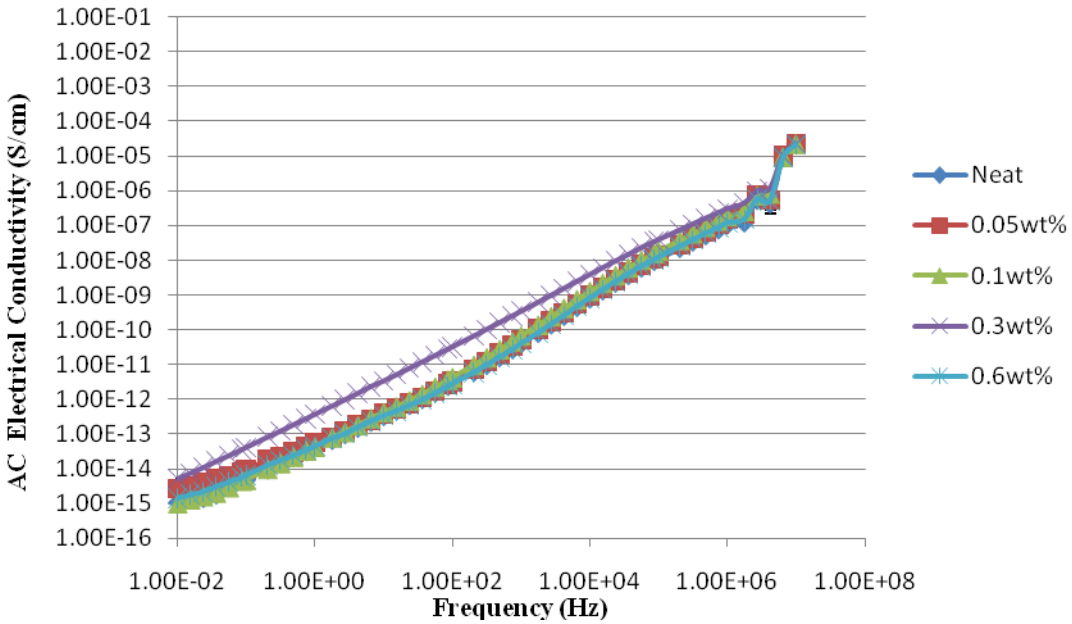

Figure 27. AC electrical conductivity vs. frequency for fluorinated XD CNT composites as a function of CNT weight fraction

The results show that the fluorinated XD CNT samples tested remain non-conductive, even at the higher CNT weight fractions. From theoretical percolation theory, these results suggest that the percolation threshold has not been reached and the composite samples have not transitioned from insulators to conductors, thus explaining the lack of increase in electrical conductivity with CNT weight fraction at low frequencies; however, the microscopic dispersion analysis performed on the fluorinated XD CNT composites, Raman imaging and SEM, in this study showed similar dispersion for the high weight fractions of fluorinated XD CNT as compared to the pristine and oxidized XD CNTs. Since a percolation network was formed in the pristine and oxidized XD CNT composites, evident in the significant increase in electrical conductivity, a similar dispersion of fluorinated XD CNTs suggests that a CNT network might have also been formed in the fluorinated XD CNT composite samples. Therefore, it would appear that if the fluorinated CNTs did form a continuous network, damage to the tubes might be too severe, which is supported by the Raman spectroscopy results. The severe damage to the tubes might be causing significant electron scattering, ultimately reducing the intrinsic electrical conductivity of the fluorinated CNTs. As supported by Raman results, the D-band, and thus damage and asymmetry in the tubes is higher in fluorinated XD CNTs than in oxidized XD CNTs, ultimately resulting in much lower electrical conductivity of the composites.

Figure 28 shows the near-DC (0.01 Hz) electrical conductivity, for the various treatments vs. CNT weight percent.

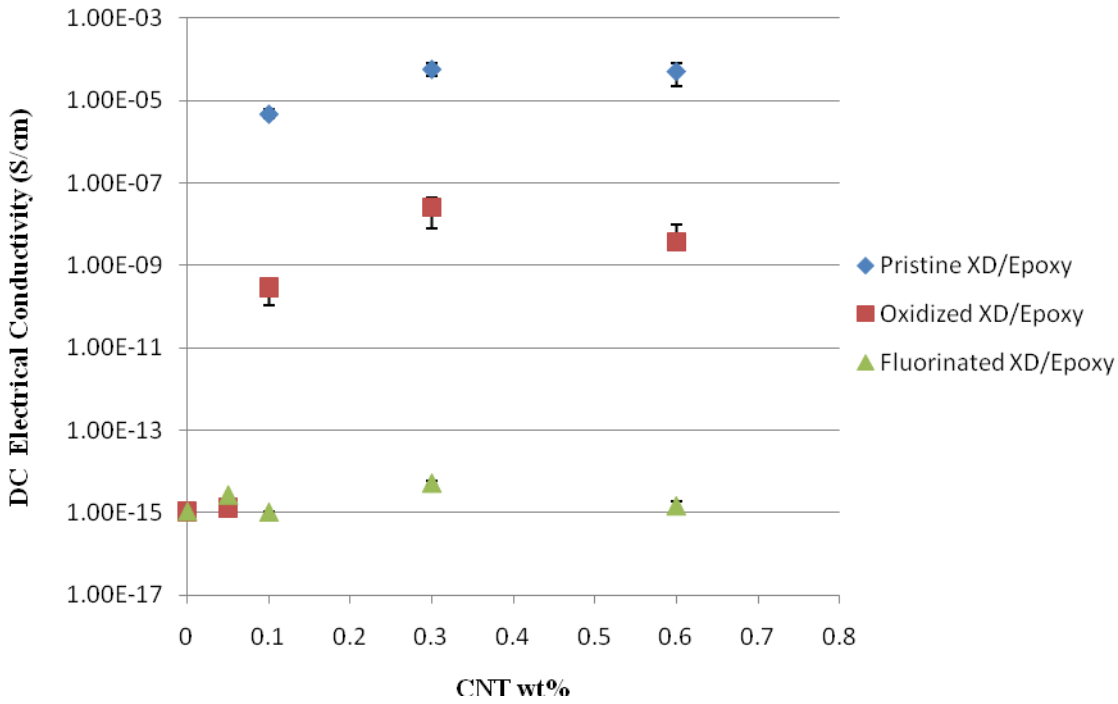

Figure 28. DC electrical conductivity as a function of CNT weight fraction for the various chemical treatments

The results show that the electrical conductivity of pristine XD CNT composites is 4 orders of magnitude higher than oxidized XD CNT samples for a 0.1 - 0.6wt% weight fraction, while the fluorinated XD CNT composites remain non-conductive. The electrical conductivity of the pristine XD CNT and the oxidized XD CNT samples show a dependence on CNT concentration with minimal change post-percolation.

As stated before, and seen again in Figure 28, the percolation threshold occurs between a weight fraction of 0.05 and 0.1 for both pristine and oxidized XD CNT

samples. In order to determine the theoretical percolation threshold, the data was fit to the power law seen in Eq. 23.

$$\sigma = A(w_f - w_{f_{perc}})^t \quad \text{for } w_f > w_{f_{perc}} \tag{23}$$

where σ is the electrical conductivity, A is a constant, w_f is the conductive filler concentration, $w_{f_{perc}}$ is the percolation concentration, and *t* is the critical exponent and a measure of dimensionality [56,62,106]. The results of the best fit power law are shown in Figure 29 and the resulting fitting parameter values shown in Table I.

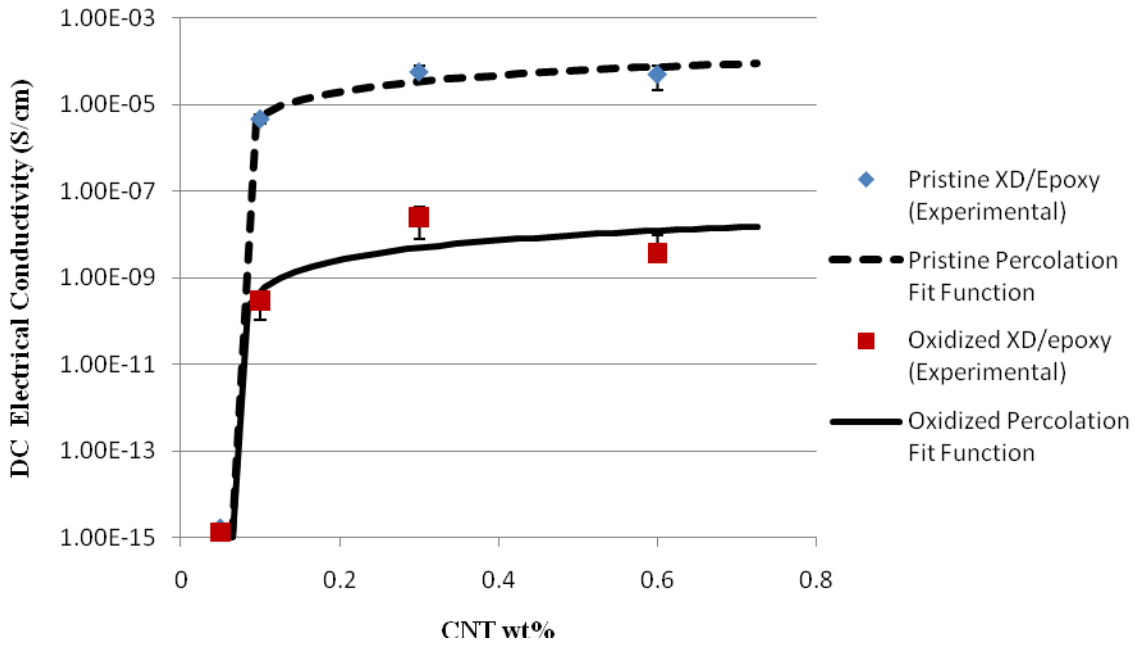

Figure 29. Percolation scaling law fit for pristine and oxidized XD CNT composites

Table I. Percolation threshold, fitted constant, and critical exponent values for pristine and oxidized XD CNT composites

Composite	$w_{f_{perc}}$ (wt%)	*A*	*t*
Pristine XD/epoxy	0.065	1.35E-4	0.95
Oxidized XD/epoxy	0.073	2.45E-8	1.09

According to the percolation power law fit, the percolation threshold for pristine and oxidized XD CNT composites have very similar values, with oxidized XD CNT composites having a slightly larger percolation threshold. This result suggests that there is a similar dispersion of CNTs for pristine and oxidized XD composites, which supports the results obtained in the dispersion analysis. Thakre et al. obtained a percolation threshold of 0.0225wt% for pristine XD CNT/epoxy composites [95]. The concentration of XD CNTs required for percolation in the study done by [95] is lower than for the study shown here, possibly due to differences in CNT dispersion. Ounaies et al. obtained a percolation threshold of 0.05 wt% for SWCNT/polyimide composites [72]. Others have shown percolation thresholds ranging from 0.007 wt% to several wt% when using SWCNTs [107]. The percolation thresholds obtained in this study are in agreement with previously reported experimental results. The exponent *t* has been shown to vary from 1.0 to 1.5 [25,72,106]. Grujicic et al. have found the critical exponent *t* to be as low as 0.87 for non-interacting CNTs [29]. Piyush et al. found a *t*

value of 1.02 for an XD CNT/epoxy composite [95]. The *t* values obtained in this study are in agreement with the values obtained from [61] for the same material system.

The differences in the percolation value, the constant *A*, and the critical exponent *t* from other published results might be due to a couple of reasons. According to [61], the percolation threshold depends on various factors such as the aspect ratio of the inclusion, the structure of the CNT bundles, size effects, and entanglements and contacts between CNTs. These factors might explain why there are some variations in percolation threshold values reported in literature. In an ideal case, the constant *A* should yield the electrical conductivity of the CNT. However, the magnitude of this constant can deviate from the electrical conductivity of the CNT. The percolation theory assumes that the CNTs are in direct contact and thus assumes that percolation is the only conduction mechanism present. The electrical conduction mechanisms in a CNT/epoxy system occur at different scales. At the nanoscale, electrical conduction within the CNTs is dominated by ballistic conduction, where electrons travel on a mean free path [47]. At the microscale, quantum tunneling, or electron hopping, describes conduction between adjacent CNTs [15,90]. If the distance between CNTs is small enough, electrons are able to tunnel quantum mechanically from one CNT to another. If the distance between the CNTs is large, a large resistance arises due to the insulating matrix between the CNTs, while with tunneling, a lower resistance results, ultimately increasing the effective conductivity of the composite [28,80]. At the macroscale, percolation is responsible for electron transport [90]. The percolation theory only considers the macroscale conduction. This theory fails to account for any other conduction

mechanisms present in these CNT composites at lower scales, such as electron hopping, and fails to account for the contact resistance between two CNTs, which can also decrease the effective electrical conductivity of the CNT [6,72]. Only considering the percolation conduction on the larger scale gives a possible reason for such a difference between the value of *A* and the conductivity of a CNT. Also, the damage caused by the oxidation of the CNTs might be the main contributor to the significant decrease in the fitted constant *A* relative to the pristine XD CNT case. According to McLachlan et al. [61], the exponent *t* is a measure of the dimensionality of the system, and the value of *t* for a CNT composite can be less than the theoretical value of an ideal 3D system (t = 2.0) due to distribution of CNT bundles. Also, there might exist a 2D system within the 3D system the controls the electrical conductivity [61].

Even though the dispersion of the pristine and oxide XD CNT composites is similar, as supported by the dispersion analysis and the similar percolation threshold, they are not completely identical. Results from the dispersion analysis show that even though the distribution of both pristine and oxidized XD CNTs is uniform, the composite samples with pristine XD CNTs show a slightly greater degree of CNT agglomeration at the microscale (Figure 18b,d), as compared to the oxidized XD CNT samples. The distribution of a greater number of agglomerates results in the agglomerates coming closer together (Figure 23b), and thus, possibly facilitating the electron hopping conduction mechanism by reducing the distance between adjacent CNTs. This result might explain the reason for the larger increase in electrical conductivity [60] for pristine XD CNT loaded samples as compared to the oxidized XD samples of the same weight

fraction. Another positive aspect of the agglomerated network is the increase in possibility of CNTs coming into direct contact and percolating, hence a possible explanation for the lower theoretical percolation threshold as compared to oxidized XD CNT composites. The dispersion of the pristine XD CNTs increases the possibility of having both conduction mechanisms, percolation by direct contact and electron tunneling, yielding different results than the oxidized XD CNT case. Also, the decrease in the magnitude of the electrical conductivity post-percolation for the oxidized XD CNT composites might be a result of damage in the oxidized tube. By oxidizing the CNT wall, the possibility of electron scattering increases since oxidizing is shown, by the Raman spectroscopy results, to introduce defects to the CNT.

The results for the AC electrical conductivity as a function of frequency for the 5 and 10 minute ball-milled pristine XD CNTs for different CNT weight fractions are shown in Figures 30 and 31, respectively.

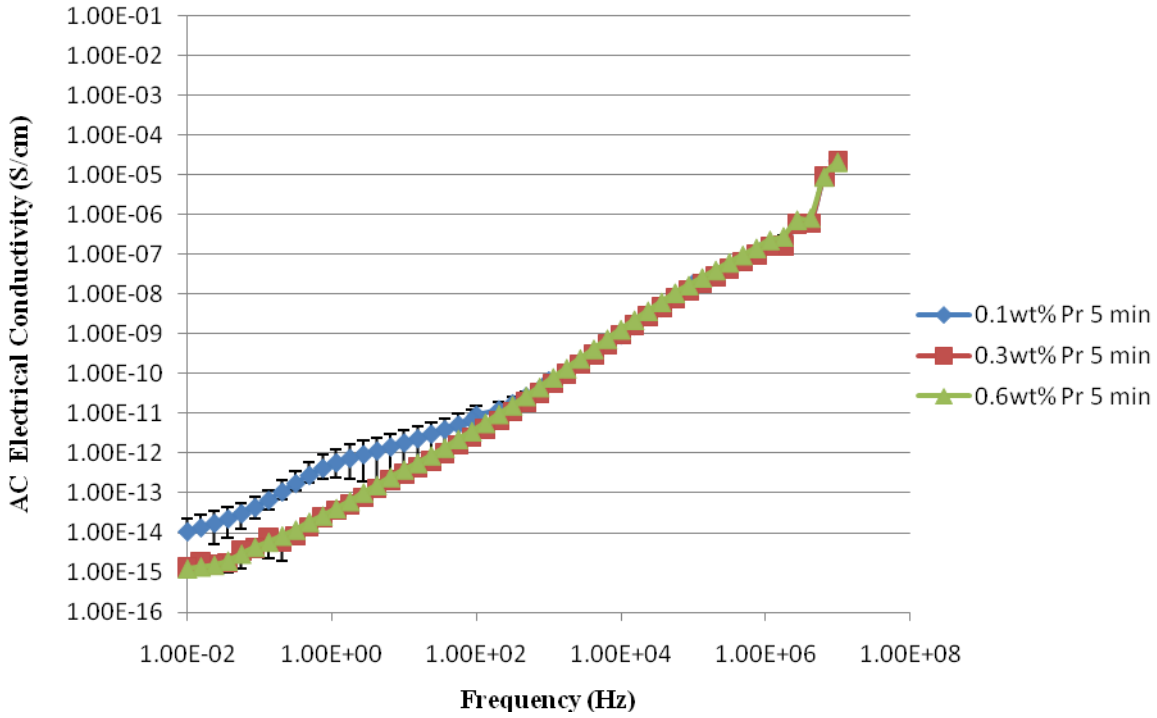

Figure 30. AC electrical conductivity vs. frequency for 5 minute ball-milled pristine XD CNT composites as a function of CNT weight fraction

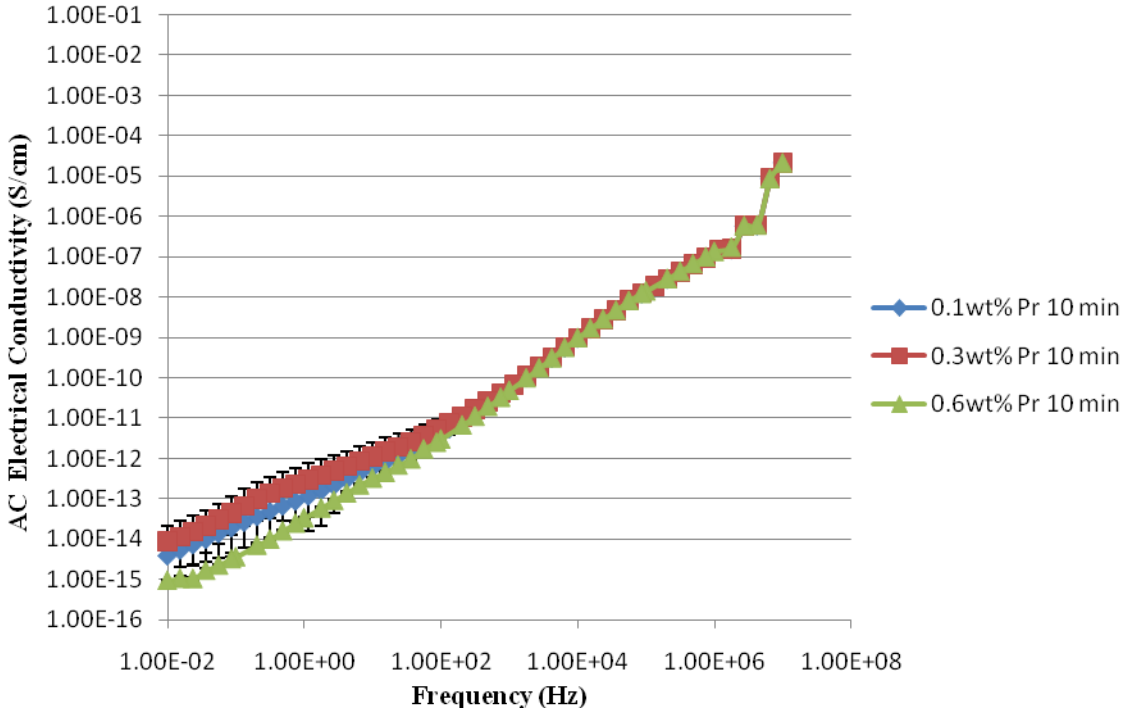

Figure 31. AC electrical conductivity vs. frequency for 10 minute ball-milled pristine XD CNT composites as a function of CNT weight fraction

Ball-milling the pristine XD CNTs significantly reduces the composite electrical conductivity, making the composite non-conductive even at the higher CNT weight fractions. One possible reason might be due to a decrease in the intrinsic electrical conductivity of the CNT by the addition of defects, as supported by Raman spectroscopy. Another reason might be due to the improvement in dispersion of CNTs. The SEM dispersion analysis shows that the agglomerates present in the ball-milled samples seem to be further apart relative to the pristine non-milled XD CNTs, making the possibility of a percolating network more difficult. There might not be enough interaction between CNTs, resulting in a lack of an electron hopping mechanism.

Therefore, a higher weight fraction of CNTs will possibly be required in order for the ball-milled CNT composites to reach a percolation threshold, making the samples electrically conductive.

D. Thermal Conductivity of XD CNT/Epoxy Composites

The thermal conductivity as a function of CNT weight fraction for pristine XD/epoxy composites is shown in Figure 32.

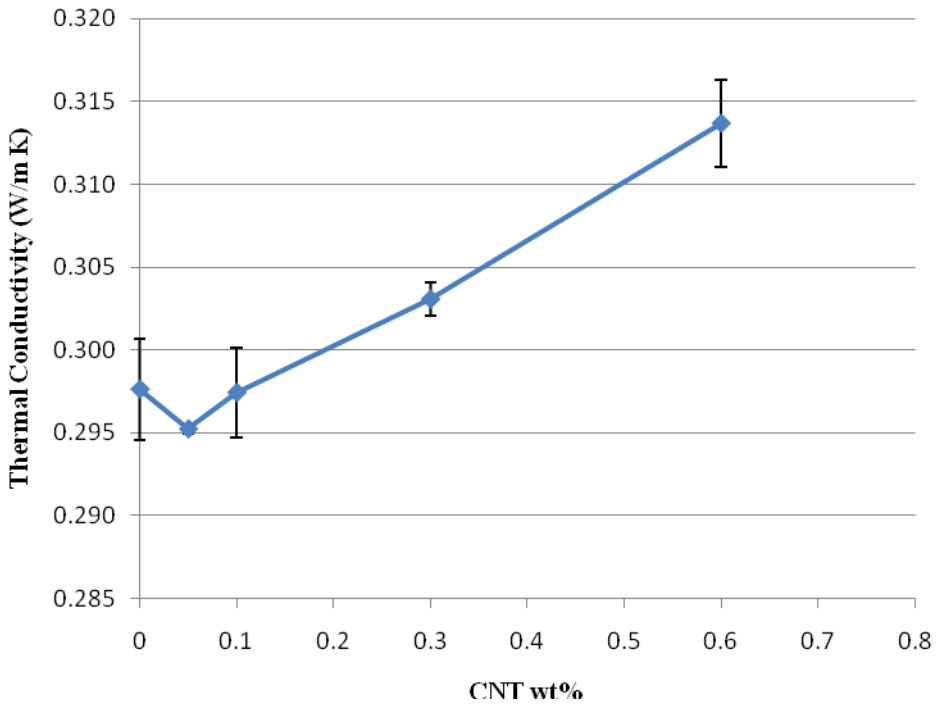

Figure 32. Thermal conductivity vs. CNT weight fraction for pristine XD CNT composites

The neat epoxy showed a thermal conductivity of 0.297 W/mK. The thermal conductivity of pristine XD CNT/epoxy composites showed an initial decrease up to 0.05wt% XD CNT, continued by a linear increase with increasing weight fraction. The thermal conductivity of pristine XD CNT at 0.6wt% increases by 5.5% relative to neat epoxy.

The results for the thermal conductivity of oxidized and fluorinated XD CNT/epoxy nanocomposites are shown in Figure 33 and Figure 34, respectively, as a function of nanotube weight fraction.

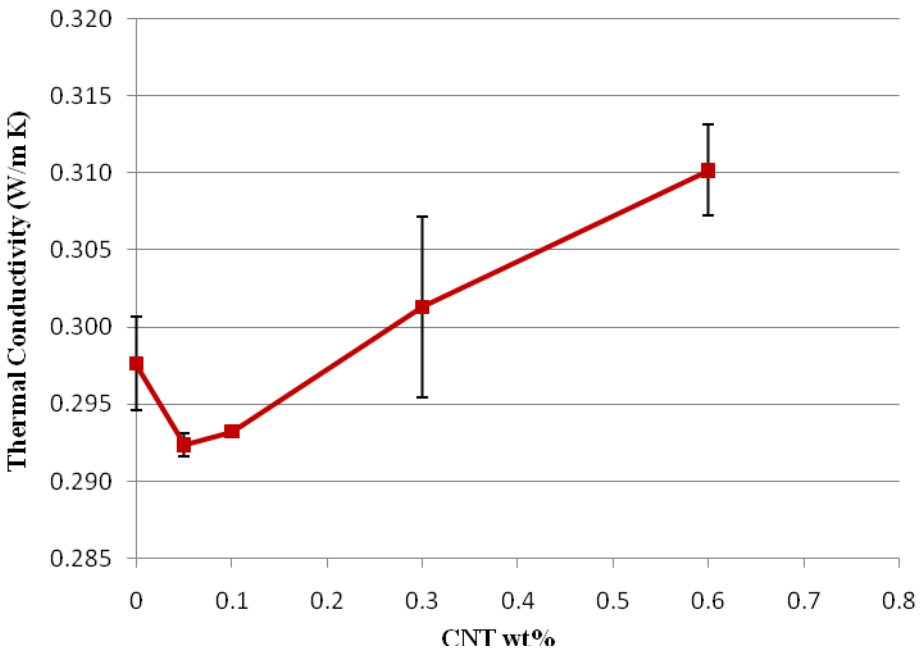

Figure 33. Thermal conductivity vs. CNT weight fraction for oxidized XD CNT composites

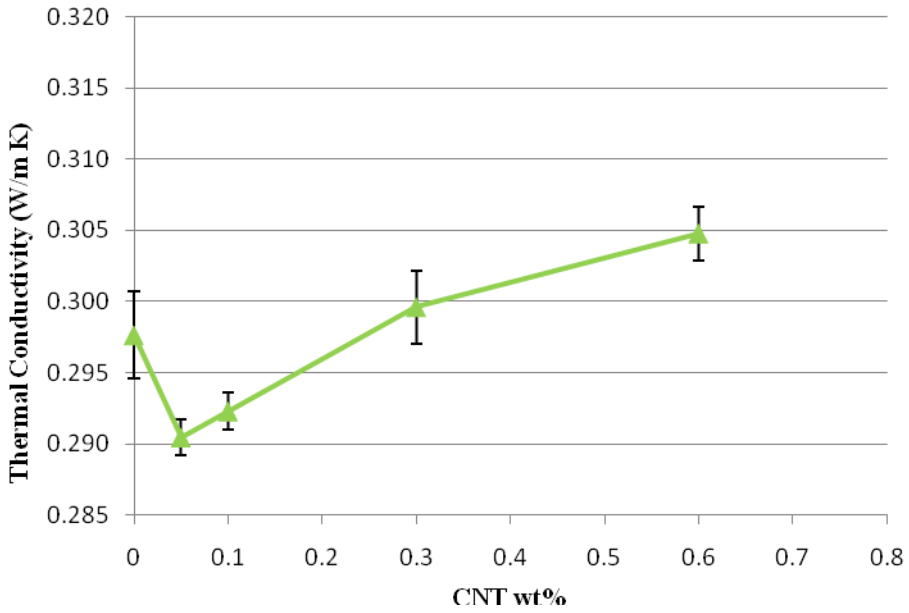

Figure 34. Thermal conductivity vs. CNT weight fraction for fluorinated XD CNT composites

At 0.6wt% oxidized XD CNT, the thermal conductivity of oxidized XD CNT/epoxy composites increases by 4.3%. For fluorinated XD CNT case, the thermal conductivity increases by 2.5% at the same CNT weight fraction of 0.6wt%. The trend observed for pristine XD composites of an initial decrease followed by a linear increase in thermal conductivity as nanotube weight fraction increases is also observed for the oxidized and fluorinated XD CNT composite samples.

In a CNT composite, the phonon frequency mismatch at the CNT/matrix interface will greatly reduce the transport of phonons, thus altering the thermal conductivity of the composite [91]. This scattering of phonons gives rise to a large thermal resistance [70,97,98]. The transport of phonons can further be altered by

functionalization of the CNTs due to the presence of more defect sites where phonons can scatter [103]. In this study, the presence of more defect sites caused by functionalization, as supported by Raman spectroscopy, might explain the reason why the thermal conductivity of the oxidized and fluorine-functionalized CNT composites is slightly lower than that of pristine CNT composites. According to Shenogin et al., as more defects are introduced into the CNT, the phonon mean free path decreases, resulting in a decrease in the intrinsic thermal conductivity of the CNT [87]. They also show that the thermal interface resistance can be decreased by functionalization due to the presence of stronger chemical bonds between the matrix and CNT, but the bonds create phonon scattering centers and thus reduce the thermal conductivity of the tube. A significant reduction in intrinsic CNT thermal conductivity caused by oxidation and fluorine-functionalization provides a possible explanation for why the results are lower than for pristine XD CNT composites. Wang et al. state that phonon vibrational modes in CNTs possess high symmetrical properties [102]. In other words, anything that breaks the symmetry of the CNT will result in phonon scattering and thus reduce phonon transport in the CNT. As shown previously by the Raman spectroscopy results of the oxidized and fluorinated XD CNTs, there is high asymmetry in the functionalized CNT structures, with fluorinated XD CNTs showing the highest intensity of asymmetry. The asymmetry in these chemically modified XD CNTs provides another possible explanation for the decrease in thermal conductivity of the composites relative to the non-modified pristine XD CNT composite case.

It has been shown that agglomerated CNTs can have significantly low thermal conductivities [11]. Therefore, the individual dispersion of the CNTs in the matrix becomes extremely important if a significant increase in thermal conductivity is to be achieved. The dispersion analysis, specifically Raman imaging and SEM, yielded results showing that agglomerates are forming in the composite samples for pristine, oxidized, and fluorinated XD CNTs. Therefore, the minimal increase in thermal conductivity may also be due to the presence of agglomerates [103].

In order to attempt to increase the thermal conductivity of the CNT/epoxy composites, the pristine XD CNTs were ball-milled in order break up the aggregates present in the supplied XD grade CNT material. The results for the ball-milled pristine XD CNT composites at two different times are shown in Figure 35 and compared to non-milled pristine XD CNT composites.

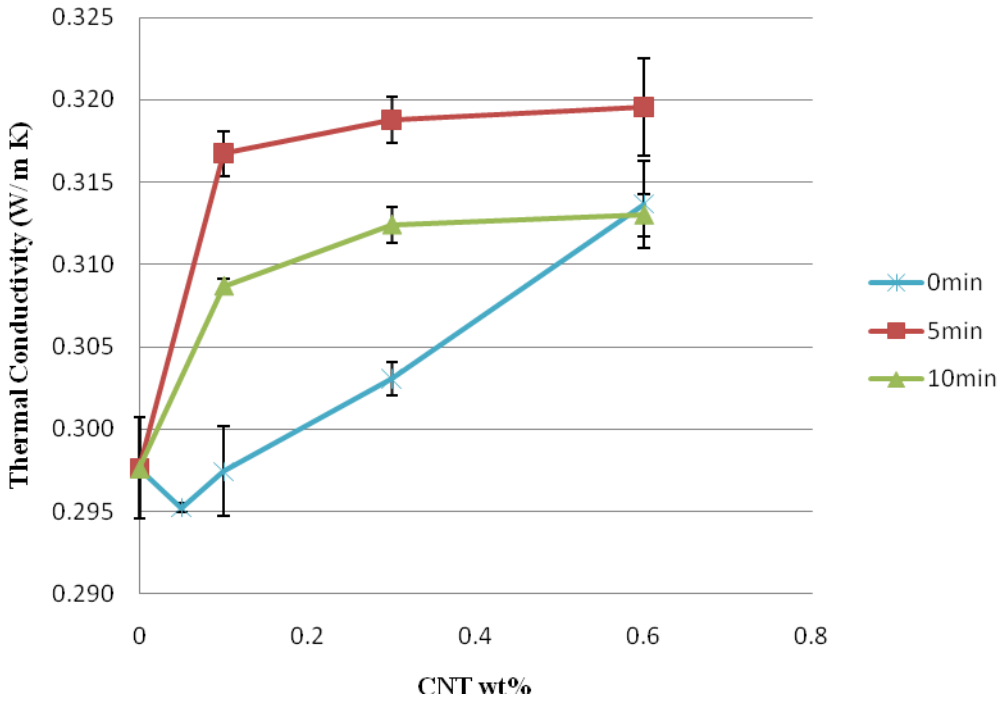

Figure 35. Thermal conductivity vs. CNT weight fraction for ball-milled pristine XD CNT composites as a function of ball-milling time

The results show that ball-milling the pristine XD CNT gives greater improvement in thermal conductivity than the untreated pristine XD CNTs, with a 6.5% increase over pure epoxy at only 0.1wt% XD CNT for a ball-milling time of 5 minutes, and 3.8% for 10 minutes. At 0.6wt%, the 5 minute ball-milled XD CNT composites show an increase of 7.5% relative to neat epoxy while the 10 minute ball-milled XD CNT composites increase by 5.3%. The same enhancement in thermal conductivity obtained at high weight fractions by non-milled pristine XD CNT composites can be obtained at much lower CNT concentrations when ball-milling the CNTs. After the

initial increase in thermal conductivity, the ball-milled XD CNT samples show minimal increase in thermal conductivity with increasing weight fraction.

The increase in thermal conductivity over non-milled pristine XD CNTs may be possibly due to a decrease in thermal resistance by the formation of smaller agglomerates. As seen in the SEM dispersion analysis, the ball-milled CNT samples show smaller agglomerates with a greater distance between them as compared to non-milled pristine CNT composites, and thus less tube to tube contact. One interesting point to notice is that as ball milling time is increased past 5 minutes, there is a decrease in thermal conductivity enhancement. One possible reason might be the reduction in CNT length, which might decrease the intrinsic thermal conductivity of the CNT and ultimately decrease the thermal conductivity enhancement [90].

One interesting result is that the thermal conductivity of the XD CNT/epoxy composites does not reach a percolation threshold (at least not over the range of weight fractions studied), as does the electrical conductivity. Assuming the CNT electrical and thermal conductivity shown in Table II, and using the experimental values obtained for the matrix electrical and thermal conductivity, the CNT to matrix ratio of electrical and thermal conductivity is found and shown in Table II.

Table II. Thermal and electrical conductivity ratios using assumed CNT and experimental matrix conductivity values

σ_{CNT} (S/cm)	σ_{mat} (S/cm)	$\frac{\sigma_{CNT}}{\sigma_{mat}}$	k_{CNT} (W/m K)	k_{mat} (W/m K)	$\frac{k_{CNT}}{k_{mat}}$
1000	1.06e-15	9.43e17	2000	0.2973	6.73e3

A difference of about 14 orders of magnitude is observed between the electrical and thermal conductivity ratios. According to Shenogina et al., the high electrical conductivity ratio makes the percolating network more efficient for electron conduction while for thermal conductivity, the low ratio requires conduction to involve the matrix material [89]. Therefore, the percolation conduction mechanism might be eliminated by interfacial thermal resistance, along with CNT to CNT contact resistance, since these effects are preventing the flow of heat through the percolated network [10,88,89,98,110]. In order for a percolation threshold to exist in a filler/polymer composite, the conductivity ratio between the filler and the polymer must be greater than 1e5 [63], explaining why the electrical conductivity of the composites tested here shows a percolation threshold and the thermal conductivity does not.

E. Micromechanics Modeling of CNT/Epoxy Composites

In order to obtain results using the micromechanics model, the CNT geometry input parameters, shown in Table III, were assumed [28,82]. The material properties shown in Table IV were obtained from the acquired experimental results for the epoxy matrix and from [23,44,84] and [39] for the CNT electrical and thermal conductivity, respectively. The experimental results obtained in this study were used for obtaining some modeling parameters, such as the thickness and the electrical and thermal conductivity of the interface layer. These parameters were adjusted in order for the micromechanics model to fit and correctly simulate the experimental results obtained in this study.

Table III. CNT geometry parameters for input into micromechanics model

r_{CNT} (nm)	r_0 (nm)	l_{CNT} (μm)	Aspect Ratio
1	0.66	3	1500

Table IV. Epoxy and CNT electrical and thermal conductivity

σ_{mat} (S/cm)	σ_{CNT} (S/cm)	k_{mat} (W/m K)	k_{CNT} (W/m K)
1.06e-15	1000	0.2973	2000

1. Electrical Conductivity Modeling Results

The electrical conductivity modeling results for the CNT/epoxy composites using a composite cylinders method are shown in Figure 36.

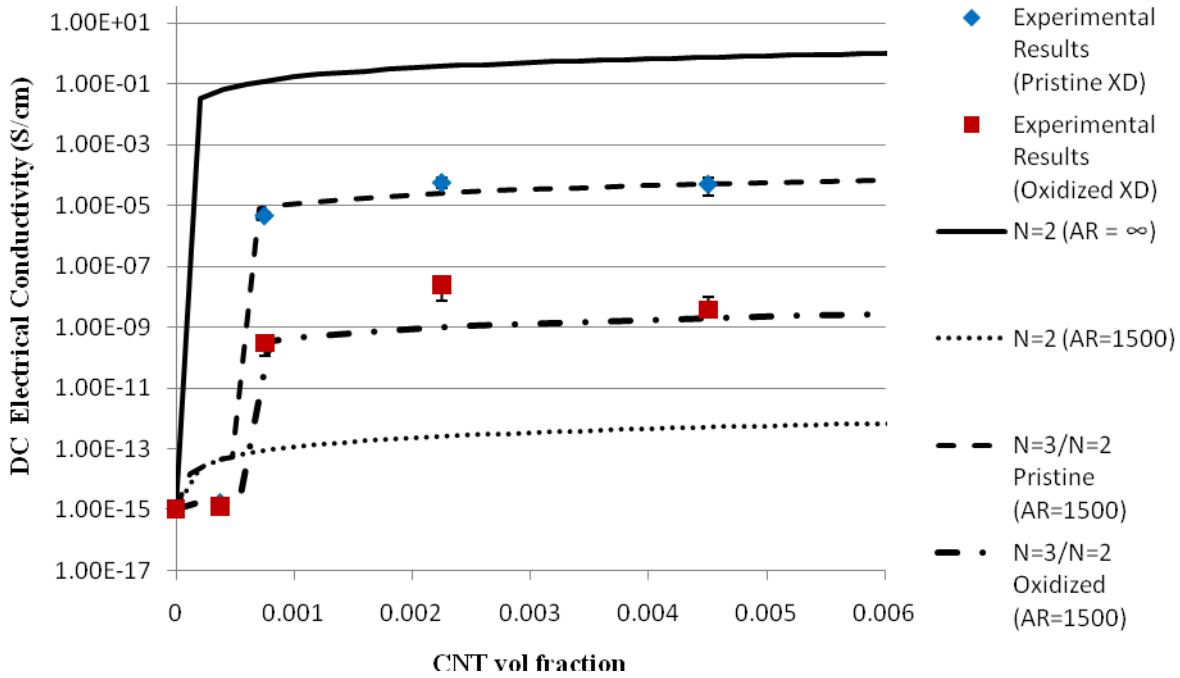

Figure 36. Micromechanics electrical conductivity modeling results compared to experimental results

As seen in Figure 36, when the interface layer is not considered (N=2), the electrical conductivity of the composite does not reach a percolation threshold. The lack of percolation might possibly be due to the high resistance provided by the matrix. Since with an N=2 assemblage there is always matrix material between adjacent CNTs, the increase in electrical conductivity is only slight and very large volume fractions are required to reach the electrical conductivity values of the experimental results.

As seen in Figure 36, when using an N=2 assemblage, the electrical conductivity of this assemblage is only increased by increasing the aspect ratio of the CNT. A finite

aspect ratio, as with the experimental results, will yield only minimal increase of about 2 or 3 orders of magnitude at the volume fractions used for the fabricated samples. An aspect ratio of infinity gives electrical conductivity values much greater than those of the experimental results. The N=2 approach fails to accurately simulate the experimental results possibly due to this approach lacking the conduction mechanism from CNT to CNT and only considering ballistic electron conduction within the CNTs.

In order to correctly simulate the experimental results, an electron hopping layer was considered. When considering electron hopping, the composite cylinder assemblage consists of three phases (N=3), the CNT, the electron hopping interface, and the matrix. Using the percolation threshold results obtained from the percolation scaling law shown in Table I, the thickness of the electron hopping interface layer is calculated. First, the percolation threshold weight fraction is converted to volume fraction by the use of Eq. 24 and an epoxy density, $\rho_{epoxy} = 1.2$ g/cm^3 [36] and a CNT density taken as, $\rho_{CNT} = 1.6$ g/cm^3 [101].

$$v_f = \frac{\rho_{epoxy} w_f}{\rho_{CNT}(1-w_f)+\rho_{epoxy} w_f} \tag{24}$$

The percolation threshold obtained from the experimental results in this study, $v_{f_{perc}}$, corresponds to the transition from an N=3 to an N=2 cylinder assemblage [82,84], when there is no matrix material between adjacent CNTs and a conductive path is formed, not by physical contact but by electron hopping. The critical volume fraction, v_c, corresponding to this transition is shown in Eq. 25. The thickness of the electron

hopping interface layer, t_{int}, is then calculated and the final result shown in Table V for both the pristine and oxidized XD CNT cases.

$$v_c = v_{f_{perc}} = \frac{r_{CNT}^2}{(r_{CNT}+t_{int})^2} \tag{25}$$

Table V. Percolation threshold and CNT interface layer parameters

Composite	$w_{f_{perc}}$ (wt frac)	$v_{f_{perc}}$ (vol frac)	t_{int} (nm)	σ_{int} (S/cm)
Pristine XD/epoxy	0.00065	0.00049	44.27	1.0e8 $\cdot \sigma_{mat}$
Oxidized XD/epoxy	0.00073	0.00055	41.72	1.0e4 $\cdot \sigma_{mat}$

The conductivity of the interface layer, σ_{int}, was adjusted to best fit and most accurately simulate the experimental data as shown in Figure 36. From the modeling results obtained, it can be concluded that the interface thickness governs at what volume fraction the percolation threshold takes place. Electron hopping can range between 26-80 nm [14,111]. The result for the interface thickness obtained in this study lies well within this range which further highlights the fact that electron hopping dominates the electrical conduction in our CNT/epoxy system.

As seen in the results, there is an increase in electrical conductivity with an increase in volume fraction before the percolation threshold when considering an N=3 assembly. As volume fraction increases, the matrix material between adjacent CNT/interface cylinders decreases and thus the effective electrical conductivity of the

composite increases. This increase in effective electrical conductivity is possibly due to the decrease in resistance from the lack of matrix material between adjacent CNTs. As volume fraction continues to increase, the matrix between adjacent CNT/interface further decreases until a point where there is no matrix material between the CNT/interface and the interface layers come into contact, initializing the electron hopping mechanism. At the point where the interface layers come into contact, there is a sharp increase in electrical conductivity due to both the lack of resistance from the matrix and the electron hopping conduction mechanism, forming a conductive network within the composite material.

Post percolation, the electrical conductivity of the composite is dominated by the magnitude of the conductivity of the interface layer. As seen in the experimental results, the electrical conductivity of the oxidized XD CNT/epoxy composites is 4 orders of magnitude lower than that of the pristine XD CNT/epoxy composites. The same difference in magnitude is observed in the electrical conductivity of the modeled interface layer as shown in Table V. The lower electrical conductivity of the interface layer suggests that the electron hopping mechanism in oxidized CNTs is not as effective as in pristine CNTs. This suggestion might explain why the experimental electrical conductivity of the oxidized XD CNT composites is lower relative to pristine XD CNT composites. One possibility might be that with oxidized CNTs, there is a decrease in electron hopping likely due to the presence of more defects, as is supported by experimental Raman spectroscopy results, created by the oxidation process.

2. Thermal Conductivity Modeling Results

The thermal conductivity modeling results for the pristine CNT/epoxy composites are shown in Figure 37.

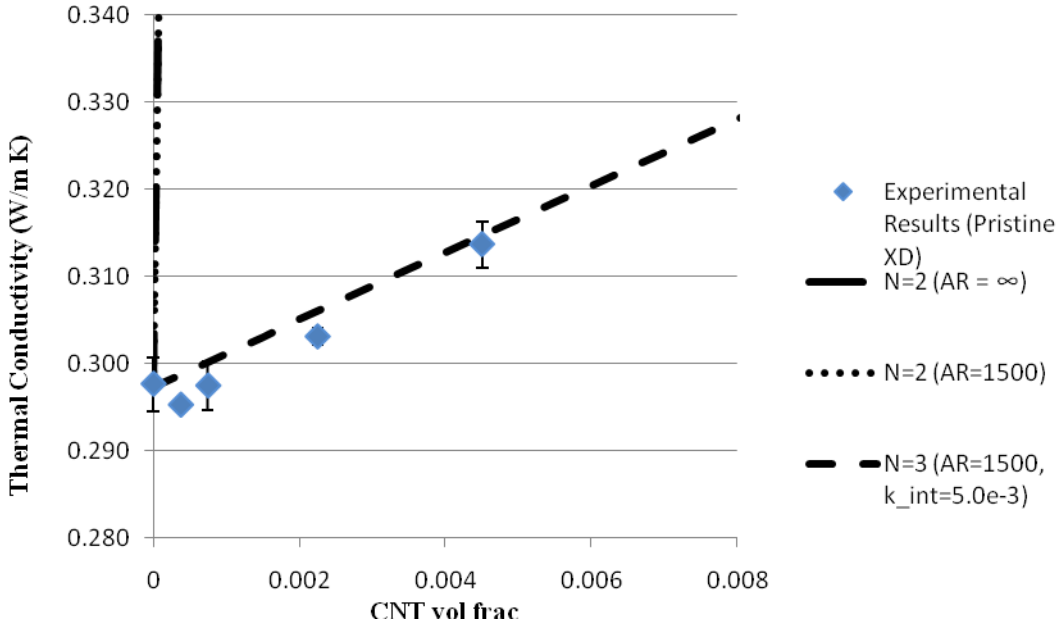

Figure 37. Micromechanics thermal conductivity modeling results compared to experimental results for pristine CNT composites

The modeling results show that by not considering an interface between the CNT and matrix, thermal conductivity values for the composite much greater than the experimental results are obtained. By not considering an interface layer, the scattering of phonons is not present and therefore the high intrinsic thermal conductivity of the individual CNTs leads to a high thermal conductivity. Also, a finite aspect ratio does not affect the thermal conductivity of the N=2 assemblage since end effects are not taken

into consideration. Therefore, the N=2 approach fails to accurately simulate the experimental results possibly due to not considering the interface thermal resistance, resulting from the phonon frequency mismatch between the CNT and matrix [88,107].

To accurately simulate the experimental thermal conductivity results, the interface thermal resistance was considered. When using the N=3 composite cylinder assemblage, the three phases considered are the CNT, a thermal resistance interface, and the matrix. Seidel et al. used a value of 0.3 nm for an interface thickness between a CNT and a polyethylene matrix in order to account for imperfect load transfer [83]. The same value for the interface thickness was used here when modeling the N=3 assemblage. The thermal conductivity of the interface layer, k_{int}, was adjusted, to the value shown in Table VI, to yield the best fit and provide the best simulation of the experimental data. As shown in Figure 37, the N=3 approach fits the experimental data well, suggesting the thermal conductivity in XD CNT/epoxy composites is dominated by the high thermal resistance of the interface.

Table VI. Thickness and thermal conductivity of CNT/epoxy interface for pristine CNT composites

Composite	t_{int} (nm)	k_{int} (W/m K)
Pristine CNT/epoxy	0.3	5.0e-3

The thermal conductivity of the oxidized and fluorine-functionalized CNT/epoxy composites is simulated in Figure 38.

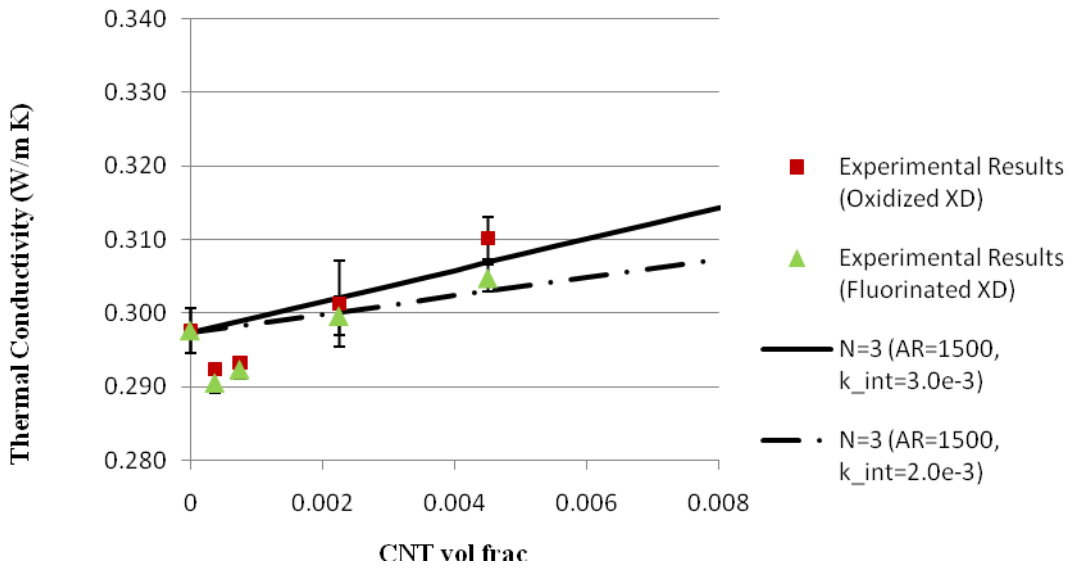

Figure 38. Micromechanics thermal conductivity modeling results compared to experimental results for oxidized and fluorine-functionalized CNT composites

For simplicity, it is assumed that the interface thickness remains the same for pristine, oxidized, and fluorinated CNTs. The parameter values for the thermal conductivity and thickness of the interface that yield the best fit to experimental results are shown in Table VII.

Table VII. Thickness and thermal conductivity of CNT/epoxy interface for oxidized, and fluorinated CNT composites

Composite	t_{int} (nm)	k_{int} (W/m K)
Oxidized CNT/epoxy	0.3	3.0e-3
Fluorinated CNT/epoxy	0.3	2.0e-3

As shown in Table VII, the thermal conductivity of the interface decreases with oxidized and fluorinated XD CNTs. The interface region accounts for reduced phonon transport resulting from the CNT/epoxy phonon frequency mismatch. The interface conductivity results suggest that phonon transfer through the interface decreases with functionalization. The model does fails to predict the initial decrease observed in the oxidized and fluorinated XD CNT composite samples.

Shenogin et al. [88] suggest that a stronger coupling, by functionalization, between the CNT and matrix will reduce the thermal interface resistance, contrary to the modeling results obtained above. However, [88] states that the intrinsic thermal conductivity of the CNT will be severely reduced, which was not considered in the results in Figure 38. Therefore, the reduction of the intrinsic thermal conductivity of the CNT, by scattering of phonons, is considered and the parameter values yielding the best fit to experimental results shown Table VIII and the simulated results shown Figure 39.

Table VIII. Thermal conductivity of CNT and CNT/epoxy interface for oxidized, and fluorinated CNT composites when accounting for reduction in intrinsic CNT thermal conductivity

Composite	k_{CNT} (W/m K)	k_{int} (W/m K)
Oxidized CNT/epoxy	25.0	7.0e-3
Fluorinated CNT/epoxy	15.0	8.0e-3

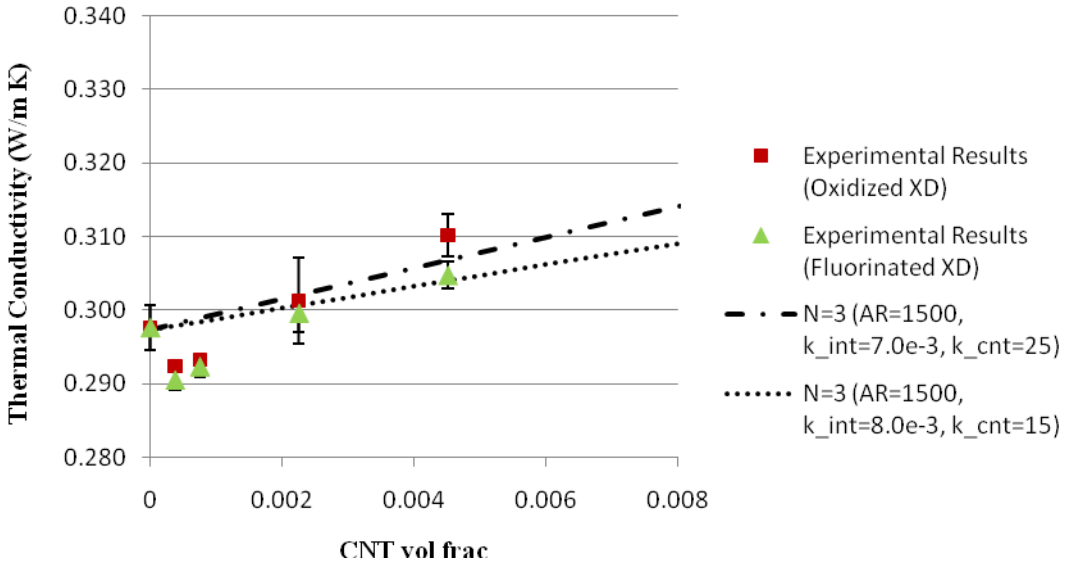

Figure 39. Micromechanics thermal conductivity modeling results compared to experimental results for oxidized and fluorine-functionalized CNT composites accounting for decrease in CNT intrinsic conductivity

The results in Figure 39 are almost identical to the results shown in Figure 38. The agreement is due to the similarity in the effective thermal conductivity of the total CNT/interface assemblage, even though the thermal conductivities of the CNT and of the interface themselves are different. As shown in Table VIII, the thermal conductivity of the interface region can be higher for the oxidized and fluorinated XD CNT composites relative to the pristine XD CNT composites, but a significant reduction in the thermal conductivity of the CNT is observed, with fluorination resulting in a higher reduction than oxidation. This result is supported by the Raman spectroscopy results showing and increase in defects and asymmetry with functionalization, both which act to scatter phonons, reducing the thermal conductivity of the CNT, with fluorinated XD CNTs having a higher intensity than oxidized XD CNTs. The modeling results obtained when considering the decrease in intrinsic thermal conductivity of the CNT are supported by Shenogin et al., where they found that chemical bonding of a CNT to a matrix reduces the thermal interface resistance while decreasing the CNT thermal conductivity [87]. The significant reduction in intrinsic thermal conductivity of the CNT will ultimately decrease the thermal conductivity of the composite material. One important point to notice is that while the thermal conductivity of the CNT decreased significantly, the thermal conductivity of the interface only increased slightly. This again emphasizes the importance the interface has on the overall thermal conductivity of the composite and how the composite thermal conductivity is dominated by the thermal interface resistance.

CHAPTER IV

CONCLUSIONS AND FUTURE WORK

This work has shown the effect of CNT nanoconstituents on the thermal and electrical properties of epoxy composites. A simple and efficient fabrication method has been used. It was found that pre-curing of the epoxy and increasing the stirring rate help to improve the distribution of XD CNT agglomerates. A qualitative analysis on the degree of dispersion was performed at different length scales by the use of different techniques. It was found that pristine XD CNTs are uniformly dispersed but some agglomeration is still present, while oxidized XD CNTs yield slightly improved dispersion. Fluorinated XD CNTs also show a uniform CNT agglomerate distribution. Therefore, when using this fabrication method, functionalization of XD CNTs does not significantly improve their dispersion. Ball-milling of CNTs effectively decreased the size of the micrometer sized aggregates present in the supplied XD CNT material. Ball-milled pristine XD CNTs yielded improved results in dispersion, with a decrease in agglomerate size and an increase in uniformity.

The electrical conductivity of the fabricated composites was determined as a function of frequency. Results show that electrical conductivity increases by 9 and 5 orders of magnitude for the pristine and oxidized XD CNT composites relative to the neat epoxy matrix, respectively, while fluorinated XD CNT composites remain electrically non-conductive. Also, pristine and oxidized XD CNT composites showed a similar percolation threshold. The electrical conductivity of the ball-milled pristine XD

CNT composites remains electrically non-conductive, possibly due to the lack of a percolation threshold. As shown by the results, the introduction of defect sites to the CNT, by oxidation, fluorine-functionalization, or ball-milling, possibly reduces the electrical conductivity of the CNT/epoxy composites.

The thermal conductivity of these CNT composites was also characterized. Thermal conductivity results show minimal increase for pristine, oxidized, and fluorinated XD CNT composites showing a linear increase in thermal conductivity with CNT weight fraction. The small increase in thermal conductivity is possibly due to the high interface thermal resistance between the XD CNTs and epoxy. Also, the asymmetry in the oxidized and fluorinated XD CNTs might also lead to a higher degree of phonon scattering, ultimately decreasing the thermal conductivity of the composite. Ball-milled pristine XD CNTs show an initial increase in thermal conductivity higher than non-milled pristine XD CNTs. After the initial increase, there is minimal increase in thermal conductivity with increase in ball-milled XD CNT weight fraction. Increasing ball-milling time past 5 minutes results in a decrease in thermal conductivity. However, the thermal conductivity improvement remains greater than the pristine XD CNT case, except at 0.6 wt%.

In addition to experimental characterization, modeling was also employed to further understand the effect of using CNT inclusions in an epoxy matrix. A micromechanics model based on the composite cylinders method was implemented to model the electrical and thermal conductivity of the CNT/epoxy composites. Even though the mathematical equations are similar, conduction mechanisms differ greatly.

Nanoscale effects in electrical and thermal conduction, such as electron hopping and interface thermal resistance, respectively, were incorporated into the model in order to accurately simulate the acquired experimental results. The results obtained for the modeling show good agreement with acquired experimental results and verify that electron hopping and thermal interface resistance dominate conduction in these composites.

Future efforts shall be focused on improving the dispersion of CNTs. Possible methods for improving CNT dispersion are the use of enhanced high-shear stirring and higher power ultrasonication. By obtaining individually dispersed CNTs in the matrix, the contact resistance might be decreased and thus the electrical and thermal conductivities of the composites might show an increase. Improving dispersion by using non-covalent functionalization, to reduce the damage to the CNT structure and thus reduce scattering effects, might also be another method. This approach will maintain the intrinsic electrical and thermal conductivity of the CNTs. Also, using CNTs, other than an XD grade, with higher purity might be beneficial to not only dispersion but also to reduce electron and phonon scattering. Another focus might be the alignment of CNTs [42,114]. Park et al. have shown that the degree of alignment of SWCNTs in a polymer matrix can be controlled by tuning the applied electric field magnitude, frequency, and application time [73]. Therefore, an attempt to align CNTs by the use electric fields can be pursued. The alignment of the one-dimensional CNTs may result in higher conductivities in the direction of the alignment [2,17,41,46,109].

REFERENCES

[1] J.H. Ahn, H.S. Shin, Y.J. Kim, H. Chung, Structural modification of carbon nanotubes by various ball milling, Journal of Alloys and Compounds 434-435 (2007) 428-432.

[2] A. Allaoui, S. Bai, H.M. Cheng, J.B. Bai, Mechanical and electrical properties of a MWNT/epoxy composite, Composite Science and Technology 62 (2002) 1993-1998.

[3] B.J. Ash, A. Eitan, L.S. Schadler, Polymer nanocomposites with particle and carbon nanotube fillers, Dekker Encyclopedia of Nanoscience and Nanotechnology (2004) 2917-2930.

[4] S. Barrau, P. Demont, A. Peigney, C. Laurent, C. Lacabanne, DC and AC conductivity of carbon nanotubes-polyepoxy composites, Macromolecules 36 (2003) 5187-5194.

[5] W. Bauhofer, J.Z. Kovacs, A review and analysis of electrical percolation in carbon nanotube polymer composites, Composites Science and Technology 69 (2009) 1486-1498.

[6] E. Bekyarova, M.E. Itkis, N. Cabrera, B. Zhao, A. Yu, J. Gao, R.C. Haddon, Electronic properties of single-walled carbon nanotube networks, Journal of American Chemical Society 127 (2005) 5990-5995.

[7] S. Berber, Y. Kwon, D. Tomanek, Unusually high thermal conductivity of carbon nanotubes, Physical Review Letters 84 (20) (2000) 4613-4616.

[8] M.J. Biercuk, M.C. Llaguno, M. Radosavljevic, J.K. Hyun, A.T. Johnson, Carbon nanotube composites for thermal management, Applied Physics Letters 80 (15) (2002) 2767-2769.

[9] V. Bohac, M.K. Gustavsson, L. Kubicar, S.E. Gustafsson, Parameter estimations for measurements of thermal transport properties with the hot disk thermal constants analyzer, Review of Scientific Instruments 71 (6) (2000) 2452-2455.

[10] P. Bonnet, D. Sireude, B. Garnier, O. Chauvet, Thermal properties and percolation in carbon nanotube-polymer composites, Applied Physics Letters 91 (2007) 1-3.

[11] Y. Chalopin, S. Volz, N. Mingo, Upper bound to the thermal conductivity of carbon nanotube pellets, Journal of Applied Physics 105 (2009) 1-5.

[12] T. Chen, G.J. Weng, W. Liu, Effect of Kapitza contact and consideration of tube-end transport on the effective conductivity in nanotube-based composites, Journal of Applied Physics 97 (2005) 1-4.

[13] Z. Chen, K. Kobashi, U. Rauwald, R. Booker, H. Fan, W.F. Hwang, J.M. Tour, Soluble ultra-short single-walled carbon nanotubes, Journal of American Chemical Society 128 (2006) 10568-10571.

[14] E.S. Choi, J.S. Brooks, D.L. Eaton, M.S. Al-Haik, M.Y. Hussaini, H. Garmestani, D. Li, K. Dahmen, Enhancement of thermal and electrical properties of carbon nanotube polymer composites by magnetic field processing, Journal of Applied Physics 94 (9) (2003) 6034-6039.

[15] S.A. Curran, D. Zhang, W.T. Wondmagegn, A.V. Ellis, J. Cech, S. Roth, D.L. Carroll, Dynamic electrical properties of polymer-carbon nanotube composites: Enhancement through covalent bonding, Journal of Materials Research 21 (4) (2006) 1071-1077.

[16] F. Deng, Q. Zheng, An analytical model of effective electrical conductivity of carbon nanotube composites, Applied Physics Letters 92 (2008) 1-3.

[17] F. Deng, Q. Zheng, L. Wang, Effects of anisotropy, aspect ratio, and nonstraightness of carbon nanotubes on thermal conductivity of carbon nanotube composites, Applied Physics Letters 90 (2007) 1-3.

[18] F. Du, C. Guthy, T. Kashiwagi, J.E. Fischer, K.I. Winey, An infiltration method for preparing single-wall nanotube/epoxy composites with improved thermal conductivity, Journal of Polymer Science: Part B: Polymer Physics 44 (2006) 1513-1519.

[19] F. Du, R.C. Scogna, W. Zhou, S. Brand, J.E. Fischer, K.I. Winey, Nanotube networks in polymer nanocomposites: Rheology and electrical conductivity, Macromolecules 37 (2004) 9048-9055.

[20] E. Dujardin, T.W. Ebbesen, A. Krishnan, M.M.J. Treacy, Purification of single-shell nanotubes, Advanced Materials 10 (8) (1998) 611-613.

[21] C.A. Dyke, J.M. Tour, Covalent functionalization of single-walled carbon nanotubes for materials applications, Journal of Physical Chemistry 108 (51) (2004) 11151-11159.

[22] T.W. Ebbesen, Carbon nanotubes, Annual Reviews Material Science 24 (1994) 235-264.

[23] T.W. Ebbesen, H.J. Lezec, H. Hiura, J.W. Bennett, H.F. Ghaemi, T. Thio, Electrical conductivity of individual carbon nanotubes, Nature 382 (1996) 54-56.

[24] K.C. Etika, F.D. Jochum, P. Theato, J.C. Grunlan, Temperature controlled dispersion of carbon nanotubes in water with pyrene-functionalized poly(N-cyclopropylacrylamide), Journal of American Chemical Society 131 (2009) 13598-13599.

[25] M. Foygel, R.D. Morris, D. Anez, S. French, V.L. Sobolev, Theoretical and computational studies of carbon nanotube composites and suspensions: Electrical and thermal conductivity, Physical Review B 71 (2005) 1-8.

[26] R. Gangopadhyay, A. De, Conducting polymer nanocomposites: A brief overview, Chemistry of Materials 12 (2000) 608-622.

[27] C. Gao, C.D. Vo, Y.Z. Jin, W. Li, S.P. Armes, Multihydroxy polymer functionalized carbon nanotubes: Synthesis, derivatization, and metal loading, Macromolecules 38 (2005) 8634-8648.

[28] F.H. Gojny, M. H. G. Wichmann, B. Fiedler, I. A. Kinloch, W. Bauhofer, A. H. Windle, K. Schulte, Evaluation and identification of electrical and thermal conduction mechanisms in carbon nanotube/epoxy composites, Polymer 47 (2006) 2036-2045.

[29] M. Grujicic, G. Cao, W.N. Roy, A computational analysis of the percolation threshold and the electrical conductivity of carbon nanotubes filled polymeric materials, Journal of Materials Science 39 (2004) 4441-4449.

[30] S.E. Gustafsson, Transient plane source techniques for thermal conductivity and thermal diffusivity measurements of solid materials, Review of Scientific Instruments 62 (3) (1991) 797-804.

[31] V.G. Hadjiev, D.C. Davis, D.C. Lagoudas, K.L. Strong, spectroscopic imaging of polymer nanocomposites containing carbon fillers, in: Proceedings of the SAMPE Fall Technical Conference, Cincinnati Hilton Netherland Plaza, Cincinnati, Ohio, October 29-November 1, 2007.

[32] V.G. Hadjiev, S. Arepalli, P. Nikolaev, S. Jandl, L. Yowell, Enhanced Raman microprobe imaging of single-wall carbon nanotubes, Nanotechnology 15 (2004) 562-567.

[33] P.J.F. Harris, Carbon nanotube composites, International Materials Reviews 49 (1) (2004) 31-43.

[34] Z. Hashin, Thermoelastic properties and conductivity of carbon/carbon fiber composites, Mechanics of Materials 8 (1990) 293-308.

[35] Hexion EPIKURE^{TM} W Epoxy curing agents product overview. http://www.hexion.com/Products/TechnicalDataSheet.aspx?id=3950. June 10, 2010.

[36] Hexion EPON^{TM} (EPIKOTE^{TM}) Resin 862 technical data sheet. http://www.hexion.com/Products/TechnicalDataSheet.aspx?id=3950. June 10, 2010.

[37] D. Hill, Y. Lin, L. Qu, A. Kitaygorodskiy, J.W. Connell, L.F. Allard, Y.P. Sun, Functionalization of carbon nanotubes with derivatized polyimide, Macromolecules 38 (2005) 7670-7675.

[38] M. Hindermann-Bischoff, F. Ehrburger-Dolle, Electrical conductivity of carbon black-polyethylene composites experimental evidence of the change of cluster connectivity in the PTC effect, Carbon 39 (2001) 375-382.

[39] J. Hone, M. Whitney, C. Piskoti, A. Zettl, Thermal conductivity of single-walled carbon nanotubes, Physical Review B 59 (4) (1999) 2514-2516.

[40] W. Hong, N. Tai, Investigations on the thermal conductivity of composites reinforced with carbon nanotubes, Diamond & Related Materials 17 (2008) 1577-1581.

[41] H. Huang, C. Liu, Y. Wu, S. Fan, Aligned carbon nanotube composite films for thermal management, Advanced Materials 17 (2005) 1652-1656.

[42] S. Huang, L. Dai, A.W.H. Mau, Patterned growth and contact transfer of well-aligned carbon nanotube films, Journal of Physical Chemistry B 103 (1999) 4223-4227.

[43] S. Jain, P. Kang, Y. Yeo-Heung, T. He, S.L. Pammi, A. Muskin, S. Narsimhadevara, D. Hurd, M.J. Schulz, J. Chase, S. Subramaniam, V. Shanov, F.J. Boerio, D. Shi, R. Gilliland, D. Mast, C. Sloan, Building smart materials

using carbon nanotubes, in: Proceeding of The International Society for Optical Engineering (SPIE) (2004) 1-9.

[44] K. Kaneto, M. Tsuruta, G. Sakai, W.Y. Cho, Y. Ando, Electrical conductivities of multi-wall carbon nanotubes, Synthetic Metals 103 (1999) 2543-2546.

[45] I. Kang, Y.Y. Heung, J.H. Kim, J.W. Lee, R. Gollapudi, S. Subramaniam, S. Narasimhadevara, D. Hurd, G.R. Kirikera, V. Shanov, M.J. Schulz, D. Shi, J. Boerio, S. Mall, M. Ruggles-Wren, Introduction to carbon nanotube and nanofiber smart materials, Composites: Part B 37 (2006) 382-394.

[46] S.J. Kang, C. Kocabas, T. Ozel, M. Shim, N. Pimparkar, M.A. Alam, S.V. Rotkin, J.A. Rogers, High-performance electronics using dense, perfectly aligned arrays of single-walled carbon nanotubes, Nature Nanotechnology 2 (2007) 230-236.

[47] R. Khare, S. Bore, Carbon nanotube based composites-a review, Journal of Minerals and Materials Characterization and Engineering 4 (1) (2005) 31-46.

[48] B. Kim, J. Lee, I. Yu, Electrical properties of single-wall carbon nanotube and epoxy composites, Journal of Applied Physics 94 (10) (2003) 6724-6728.

[49] D. Kim, Y. Kim, K. Choi, J.C. Grunlan, C. Yu, Improved thermoelectric behavior of nanotube-filled polymer composites with poly(3,4-ethylenedioxythiophene) poly(styrenesulfonate), ACS Nano 4 (2010) 513-523.

[50] P. Kim, L. Shi, A. Majumdar, P.L. McEuen, Thermal transport measurements of individual multiwalled nanotubes, Physical Review Letters 87 (21) (2001) 1-4.

[51] Y.J. Kim, T.S. Shin, H.D. Choi, J.H. Kwon, Y. Chung, H.G Yoon, Electrical conductivity of chemically modified multiwalled carbon nanotube/epoxy composites, Carbon 43 (2005) 23-30.

[52] J.Z. Kovacs, K. Andresen, J. R. Pauls, C.P. Garcia, M. Schossig, K. Schulte, W. Bauhofer, Analyzing the quality of carbon nanotube dispersions in polymers using scanning electron microscopy, Carbon 45 (2007) 1279-1288.

[53] A. Lazarenko, L. Vovchenko, Y. Prylutskyy, L. Matzuy, U. Ritter, P. Scharff, Mechanism of thermal and electrical conductivity in polymer-nanocarbon composites, Materialwissenschaft und Werkstofftechnik 40 (4) (2009 268-272.

[54] J. Li, P.C. Ma, W.S. Chow, C.K. To, B.Z. Tang, J.K. Kim, Correlations between percolation threshold, dispersion state, and aspect ratio of carbon nanotubes, Advanced Functional Materials 17 (2007) 3207-3215.

[55] Y.B. Li, B.Q. Wei, J. Liang, Q. Yu, D.H. Wu, Transformation of carbon nanotubes to nanoparticles by ball milling process, Carbon 37 (1999) 493-497.

[56] Y.C. Li, R.K.Y. Li, S.C. Tjong, Frequency and temperature dependences of dielectric dispersion and electrical properties of polyvinylidene fluoride/expanded graphite composites, Journal of Nanomaterials (2010) 1-10.

[57] X. Liang, L. Ling, C. Lu, L. Liu, Resistivity of carbon fibers/ABS resin composites, Materials Letters 43 (2000) 144-147.

[58] P.T. Lillehei, J.W. Kim, L.J. Gibbons, C. Park, A quantitative assessment of carbon nanotube dispersion in polymer matrices, Nanotechnology 20 (2009) 1-7.

[59] C.H. Liu, H. Huang, Y. Wu, S.S. Fan, Thermal conductivity improvement of silicone elastomer with carbon nanotube loading, Applied Physics Letters 84 (21) (2004) 4248-4250.

[60] L. Liu, K.C. Etika, K. Liao, L.A. Hess, D.E. Bergbreiter, J.C. Grunlan, Comparison of covalently and noncovalently functionalized carbon nanotubes in epoxy, Macromolecular Rapid Communications 30 (2009) 627-632.

[61] D.S. McLachlan, C. Chiteme, C. Park, K.E. Wise, S.E. Lowther, P.T. Lillehei, E.J. Siochi, J.S. Harrison, AC and DC percolative conductivity of single wall carbon nanotube polymer composites, Journal of Polymer Science: Part B: Polymer Physics 43 (2005) 3273-3287.

[62] D.S. McLachlan, M.B. Heaney, Complex ac conductivity of a carbon black composite as a function of frequency, composition, and temperature, Physical Review B 60 (18) 1999 746-751.

[63] Ye.P. Mamunya, V.V. Davydenko, P. Pissis, E.V. Lebedev, Electrical and thermal conductivity of polymers filled with metal powders, European Polymer Journal 38 (2002) 1887-1897.

[64] L.M. Manocha, J. Valand, N. Patel, A. Warrier, S. Manocha, Nanocomposites for structural applications, Indian Journal of Pure & Applied Physics 44 (2006) 135-142.

[65] C.A. Martin, J.K.W. Sandler, M.S.P. Shaffer, M.-K. Schwarz, W. Bauhofer, K. Schulte, A.H. Windle, Formation of percolating networks in multi-wall carbon-

nanotube-epoxy composites, Composites Science and Technology 64 (2004) 2309-2316.

[66] E.T. Mickelson, C.B. Huffman, A.G. Rinzler, R.E. Smalley, R.H. Hauge, J.L. Margrave, Fluorination of single-wall carbon nanotubes, Chemical Physics Letters 296 (1998) 188-194.

[67] A. Moisala, Q. Li, I.A. Kinloch, A.H. Windle, Thermal and electrical conductivity of single- and multi-walled carbon nanotube-epoxy composites, Composites Science and Technology 66 (2006) 1285-1288.

[68] M. Moniruzzaman, K.I. Winey, Polymer nanocomposites containing carbon nanotubes, Macromolecules 39 (2006) 5194-5205.

[69] T. Mori, K. Tanaka, Average stress in matrix and average elastic energy of materials with misfitting inclusions, Acta Metallurgica 21 (1973) 571-574.

[70] C. Nan, G. Liu. Y. Lin, M. Li, Interface effect on thermal conductivity of carbon nanotube composites, Applied Physics Letters 85 (16) (2004) 3549-3551.

[71] C. Nan, R. Birringer, D.R. Clarke, H. Gleiter, Effective thermal conductivity of particulate composites with interfacial thermal resistance, Journal of Applied Physics 81 (10) (1997) 6692-6699.

[72] Z. Ounaies, C. Park, K. E. Wise, E. J. Siochi, and J.S. Harrison, Electrical properties of single wall carbon nanotube reinforced polyimide composites, Composites Science and Technology 63 (2003) 1637-1646.

[73] C. Park, J. Wilkinson, S. Banda, Z. Ounaies, K. E. Wise, G. Sauti, P. T. Lillehei, J. S. Harrison, Aligned single-wall carbon nanotube polymer composites using an

electric field, Journal of Polymer Science: Part B: Polymer Physics 44 (2006) 1751-1762.

[74] N. Pierard, A. Fonseca, J.F. Colomer, C. Bossuot, J.M. Benoit, G. Van Tendeloo, J.P. Pirard, J.B. Nagy, Ball milling effect on the structure of single-wall carbon nanotubes, Carbon 42 (2004) 1691-1697.

[75] V.N. Popov, Carbon nanotubes: Properties and applications, Materials Science and Engineering R 43 (2004) 61-102.

[76] H.W. Ch. Postma, M. de Jonge, Z. Yao, C. Dekker, Electrical transport through carbon nanotube junctions created by mechanical manipulation, Physical Review B 62 (16) (2000) 653-656.

[77] T. Ramanathan, F.T. Fisher, R.S. Ruoff, L.C. Brinson, Amino-functionalized carbon nanotubes for binding to polymers and biological systems, Chemistry of Materials 17 (2005) 1290-1295.

[78] R. Ramasubramaniam, J. Chen, Homogeneous carbon nanotube/polymer composites for electrical applications, Applied Physics Letters 83 (14) (2003) 2928-2930.

[79] J. Sandler, M.S.P. Shaffer, T. Prasse, W. Bauhofer, K. Schulte, A.H. Windle, Development of a dispersion process for carbon nanotubes in an epoxy matrix and the resulting electrical properties, Polymer 40 (1999) 5967-5971.

[80] J.K.W. Sandler, J.E. Kirk, I.A. Kinloch, M.S.P. Shaffer, A.H. Windle, Ultra-low electrical percolation threshold in carbon-nanotube-epoxy composites, Polymer 44 (2003) 5893-5899.

[81] C. Schmitt, M. Lebienvenu, Electrostatic painting of conductive composite materials, Journal of Materials Processing Technology 134 (2003) 303-309.

[82] G.D. Seidel, D.C. Lagoudas, A micromechanics model for the electrical conductivity of nanotube-polymer nanocomposites, Journal of Composite Materials 43 (9) (2009) 917-941.

[83] G.D. Seidel, D.C. Lagoudas, S.J.V. Frankland, T.S. Gates, Modeling functionally graded interface regions in carbon nanotube reinforced composites, in: Proceedings of the 20th ASC Technical Conference, American Society of Composites, Drexel University, Philadelphia, PA, 2005.

[84] G.D. Seidel, Micromechanics Modeling of the Multifunctional Nature of Carbon Nanotube-polymer Nanocomposites Dissertation, Texas A&M University, College Station, 2007.

[85] S. Shaikh, L. Li, K. Lafdi, J. Huie, Thermal conductivity of an aligned carbon nanotube array, Carbon 45 (2007) 2608-2613.

[86] J. Shen, W. Huang, L. Wu, Y. Hu, M. Ye, The reinforcement role of different amino-functionalized multi-walled carbon nanotubes in epoxy nanocomposites, Composites Science and Technology 67 (2007) 3041-3050.

[87] S. Shenogin, A. Bodapati, L. Xue, R. Ozisik, P. Keblinski, Effect of chemical functionalization on thermal transport of carbon nanotube composites, Applied Physics Letters 85 (12) (2004) 2229-2231.

[88] S. Shenogin, L. Xue, R. Ozisik, P. Keblinski, D.G. Cahill, Role of thermal boundary resistance on the heat flow in carbon-nanotube composites, Journal of Applied Physics 95 (12) (2004) 8136-8144.

[89] N. Shenogina, S. Shenogin, L. Xue, P. Keblinski, On the lack of thermal percolation in carbon nanotube composites, Applied Physics Letters 87 (2005) 1-3.

[90] R.D. Sherman, L.M. Middleman, S.M. Jacobs, Electron transport processes in conductor-filled polymers, Polymer Engineering and Science 23 (1983) 36-46.

[91] S. Sihn, S. Ganguli, A. Roy, L. Qu, L. Dai, Enhancement of through-thickness thermal conductivity in adhesively bonded joints using aligned carbon nanotubes, Composites Science and Technology 68 (2008) 658-665.

[92] R.C. Smith, J.D. Carey, R.J. Murphy, W.J. Blau, J.N. Coleman, S.R.P. Silva, Charge transport effects in field emission from carbon nanotube-polymer composites, Applied Physics Letters 87 (2005) 1-3.

[93] P.C. Song, C.H. Liu, S.S. Fan, Improving the thermal conductivity of nanocomposites by increasing the length efficiency of loading carbon nanotubes, Applied Physics Letters 88 (2006) 1-3.

[94] Y.S. Song, J.R. Youn, Influence of dispersion states of carbon nanotubes on physical properties of epoxy nanocomposites, Carbon 43 (2005) 1378-1385.

[95] P.R. Thakre, Y. Bisrat, D.C. Lagoudas, Electrical and mechanical properties of carbon nanotube-epoxy nanocomposites, Journal of Applied Polymer Science 116 (2010) 191-202.

[96] E.T. Thostenson, Z. Ren, T.W. Chou, Advances in the science and technology of carbon nanotubes and their composites: A review, Composites Science and Technology 61 (2001) 1899-1912.

[97] W. Tian, R. Yang, Effect of interface scattering on phonon thermal conductivity percolation in random nanowire composites, Applied Physics Letters 90 (2007) 1-3.

[98] W. Tian, R. Yang, Phonon transport and thermal conductivity percolation in random nanoparticle composites, Computer Modeling in Engineering and Sciences 24 (2) (2008) 123-141.

[99] T.M. Tritt, Thermal Conductivity: Theory, Properties, and Applications, Kluwer Academic/Plenum Publishers, New York 2004.

[100] C.H. Tseng, C.C. Wang, C.Y. Chen, Functionalizing carbon nanotubes by plasma modification for the preparation of covalent-integrated epoxy composites, Chemistry of Materials 19 (2007) 308-315.

[101] Unidym^{TM} carbon nanotubes product data sheet. http://www.unidym.com/products materials.html. June 10, 2010.

[102] J. Wang, J.S. Wang, Carbon nanotube thermal transport: Ballistic to diffusive, Applied Physics Letters 88 (2006) 1-3.

[103] S. Wang, R. Liang, B. Wang, C. Zhang, Dispersion and thermal conductivity of carbon nanotube composites, Carbon 47 (2009) 53-57.

[104] Y. Wang, J. Wu, F. Wei, A treatment method to give separated multi-walled carbon nanotubes with high purity, high crystallization and a large aspect ratio, Carbon 41 (2003) 2939-2948.

[105] G.L. Warren, L. Sun, V.G. Hadjiev, D. Davis, D. Lagoudas, H.J. Sue, B-staged epoxy/single-walled carbon nanotube nanocomposite thin films for composite reinforcement, Journal of Applied Polymer Science 112 (2009) 290-298.

[106] M. Weber, M.R. Kamal, Estimation of the volume resistivity and electrically conductive composites, Polymer Composites 18 (6) (1997) 711-725.

[107] K.I. Winey, T. Kashiwagi, M. Mu, Improving electrical conductivity and thermal properties of polymers by the addition of carbon nanotubes as fillers, MRS Bulletin 32 (2007) 348-353.

[108] X.L. Xie, Y.W. Mai, X.P. Zhou, Dispersion and alignment of carbon nanotubes in polymer matrix: A review, Materials Science and Engineering R 49 (2005) 89-112.

[109] J. Yang, S. Waltermire, Y. Chen, A.A. Zinn, T.T. Xu, D. Li, Contact thermal resistance between individual multiwall carbon nanotubes, Applied Physics Letters 46 (2010) 1-3.

[110] A. Yu, M.E. Itkis, E. Bekyarova, R.C. Haddon, Effect of single-walled carbon nanotube purity on the thermal conductivity of carbon nanotube-based composites, Applied Physics Letters 89 (2006) 1-3.

[111] J. Zhang, W. Cui, M. Juda, D. McCammon, Non-ohmic effects in hopping conduction in doped silicon and germanium between 0.05 and 1 K, Physical Review B 57 (8) (1998) 4472-4481.

[112] Q. Zhao, H. D. Wagner, Raman spectroscopy of carbon-nanotube-based composites, Philosophical Transactions of the Royal Society London A 362 (2004) 2407-2424.

[113] J. Zhu, J. Kim, H. Peng, J.L. Margrave, V. N. Khabashesku, E.V. Barrera, Improving the dispersion and integration of single-walled carbon nanotubes in epoxy composites through functionalization, Nano Letters 3 (8) (2003) 1107-1113.

[114] L. Zhu, Y. Sun, J. Xu, Z. Zhang, D.W. Hess, C.P. Wong, Aligned carbon nanotubes for electrical interconnect and thermal management, Electric Components and Technology Conference (2005) 44-50.

VITA

Name:	Frank Gardea
Address:	Texas A&M University
	Department of Aerospace Engineering
	H.R. Bright Building, Rm. 701, Ross Street - TAMU 3141
	College Station, TX 77843-3141
Email Address:	amw_99_2000@yahoo.com
Education:	B.S., Aerospace Engineering, Texas A&M University, 2008
	M.S., Aerospace Engineering, Texas A&M University, 2011